DEVELOPMENT OF AN EXPERIMENTAL TECHNIQUE TO DISTINGUISH BETWEEN INTERNAL AND EXTERNAL CONTRIBUTIONS TO DAMPING IN ROTORS

by

LIEUTENANT P. PANIGRAHI

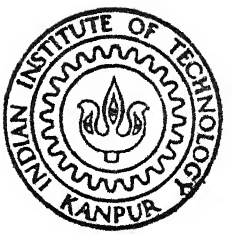

DEPARTMENT OF MECHANICAL ENGINEERING

INDIAN INSTITUTE OF TECHNOLOGY KANPUR

FEBRUARY, 1992

DEVELOPMENT OF AN EXPERIMENTAL TECHNIQUE TO DISTINGUISH BETWEEN INTERNAL AND EXTERNAL CONTRIBUTIONS TO DAMPING IN ROTORS

A Thesis Submitted
In Partial Fulfilment of the Requirements
for the Degree of
MASTER OF TECHNOLOGY

by

LIEUTENANT P. PANIGRAHI

to the

DEPARTMENT OF MECHANICAL ENGINEERING
INDIAN INSTITUTE OF TECHNOLOGY KANPUR

FEBRUARY, 1992

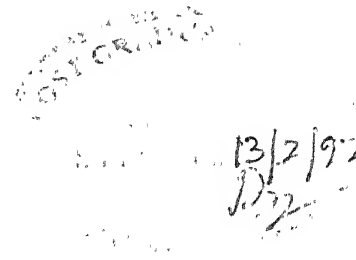

CERTIFICATE

It is certified that the work contained in this thesis entitled Development of An Experimental Technique to Distinguish Between Internal and External Contributions to Damping in Rotors by Lt. P. Panigrahi has been carried out under my supervision and that this work has not been submitted elsewhere for a degree.

February, 1992

Nalinaksh Vyas.

(Nalinaksh S Vyas)
Assistant Professor
Department of Mechanical Engineering
Indian Institute of Technology
Kanpur 208016

ACKNOWLEDGEMENTS

The work done in this thesis would not have been possible had it not been the encouragement and guidance given to me by the Dr. Nalinaksh S. Vyas. To him, I extend my heartfelt gratitude for having permitted me to work in an environment of complete freedom.

The experimental set up would not have been conceived without the enthusiastic co-operation of central workshop and manufacturing Lab. personnel. My sincere thanks are due to Mr. M.M. Singh for extending the Lab. facilities and his timely help during the course of this work.

I am indebted to Ashutosh, Prarin, Ravindranath, Rajiv, Sidharth and Rupendra for their cooperation and valuable suggestion in operating the Vib. equipments properly.

Feb. 1992. Lieutenant P. Panigrahi

CONTENT

ABSTRACT

Damping is one of the most crucial and complex parameters that determine the performance of a rotor. Rotor damping is a result of internal (intermolecular friction i.e. material hysteresis) and external (Coulomb friction at supports and gas/air environment resistance) energy dissipation mechanisms. It is essential to make a distinction between contributions from these two energy dissipation mechanisms since they affect the rotor behaviour in different ways.

In this study an experimental technique is developed for 'Separate' estimation of the internal and external damping parameters of a rotor.

A rotor test rig is fabricated. The transient polar plot of the system is experimentally obtained. Subsequently the known analytical equations governing the rotor whirl are modelled to make a distinction between the contributions from internal and external damping mechanism.

Damping is analysed as a function of whirling mode, rotor speed and whirling amplitudes.

NOMENCLATURE

C_e = External damping coefficient

C_i = Internal damping coefficient

x, y = Displacement in vertical and horizontal directions

$\dot{x}, \dot{y}$ = Velocity is vertical and horizontal directions

$\dot{x}_o, \dot{y}_o, \dot{x}_o, \dot{y}_o$ = Initial conditions for displacement and velocity in vertical and horizontal directions

r = Amplitude of whirl

r_o = Amplitude of whirl at time t = 0

G_1 = (g_1/x_o) = Non-dimensional error in vertical direction

G_2 = (g_2/x_o) = Non-dimensional error in horizontal directio

Y_o = (y_o/x_o) = Non dimensional initial displacement in horizontal direction.

X_1 = $(\dot{x}_o/x_o)$ = Non dimensional initial velocity in vertical direction

Y_1 = $(\dot{y}_o/x_o)$ = Non dimensional initial velocity in horizontal direction

X = (x/x_o) Non dimensional displacement in vertical direction after time t

Y = (y/x_o) Non dimensional displacement in horizontal direction after time t

T	=	$(p \times t)$ = Non dimensional time
P_d or P	=	The damped natural frequency in rad/sec
P_1	=	(ω/p) = Frequency ratio
ω	=	the rotational speed in rad/sec
α_{ij}	=	Influence Coefficient.

LIST OF FIGURES

CHAPTER I

INTRODUCTION

The need for higher speed, yet reliable operation of rotating machinery continues to increase. The key factor in development of high performance rotor is the ability to accurately predict the dynamic response and stability of the system in the design stage. Damping is one of the most crucial parameters that define the dynamic behaviour of the machine as well as its susceptibility to self-excited vibrations leading to instability.

The three primary damping mechanisms influencing the rotor performance are i) Viscous damping due to the surrounding gas medium, ii) friction damping at various component functions along the rotor, most frequently at the bearings and between the hub of the disc and the shaft, iii) material hysteresis or hysteretic damping which is caused by the intermolecular forces in the material arising as a result of the rate of deformation in the elastic shaft. Mechanism (i) is an external source of damping, while mechanisms (ii) and (iii) are categorised as internal sources. Unlike stationary machines where the total damping in the system is taken as the direct summation of the contributions from various damping mechanisms, in rotating machines these mechanisms affect the rotor behaviour in different ways.

Different sets of values of the internal and external damping parameters lead to either stable or unstable rotor behaviour, the unstable speed regime being defined by their relative magnitudes. Therefore, while in stationary machines it is sufficient to estimate the total effect of these damping mechanisms, in rotating machines it is essential that their contributions are known separately.

Conventional methods of obtaining the damping values from the logarithmic decrement of free vibration signals of machines can not distinguish between the contributions from internal and external sources. In this study it is proposed to develop an experimental method for separate determination of external and internal damping values for a rotor. It is also proposed to define damping as a function of whirling mode, rotor speed and whirling amplitudes to refine the existing analytical models for stability predictions.

1.1 LITERATURE SURVEY

A number of authors have dealt the problem of unstable shaft behaviours due to the self excited mechanisms of internal damping at rotational speeds above the first critical. In these studies analytical models have been developed to study internal damping arising due to both material hysteresis as well as rubbing friction at various functions across the rotor. The stability criteria have been established by comparing the internal (i.e. destabilising) damping forces with the external (i.e. stabilising)

damping forces. Analytical expressions defining unstable rotor speed regimes in terms of the relative magnitudes of internal and external damping parameters have been obtained.

The problem of unstable shaft behaviours due to self excited mechanisms of internal damping at rotational speeds above the first critical speed was detected as early as 1924 by Newkirk [1] and Kimball [2,3].

Since then attempts have been made to study this tendency towards self excited vibrations. Ehrich [4,5] analysed the important role of dry friction and internal damping in inducing the instability in rotating systems. The rotational speed at which instability occurs is governed by the ratio of external friction to internal friction.

Begg [6] developed an analysis showing that the regime of stability does exist and the induced whirling may propagate, persist or decay when the disturbance causing the whirl is removed, depending upon the frequency to damping ratio and upon the magnitude of initial disturbance.

Bansal and Kirk [7] described an analytical method based on transfer matrix approach to calculate the damped critical speeds and instability threshold speed of multimass rotor bearing systems. The effect of bearing as well as bearing support flexibility on the stability of the rotor system were discussed.

Zorzi and Nelson [8] through finite element approach investigated the effect of axial torque on the lateral dynamics of

rotor bearing systems. Glasgow and Nelson [9] presented the stability analysis of rotor bearing system and developed a method for significant reduction in the size of the overall system problems while retaining the essential dynamics characteristics.

1.2 PRESENT STUDY

The analytical tools for prediction of rotor behaviour, discussed in the previous section, do however, require numerical estimates of the internal and external damping properties of the specific rotor. In the present study an attempt has been made in the direction of estimation of these damping parameters.

The problem is defined and the derivation of the governing equation is briefly reviewed in Chapter 2. The free vibration solution to the equation is obtained and reformatted to describe the technique to extract information about the internal and external damping.

Chapter 3 describes the experimental rig and subsequent investigations. The technique is validated and results are discussed.

Chapter 4 summarises the present investigations and outlines the scope and possibilities of future attempts.

CHAPTER II

EQUATION OF MOTION AND RESPONSE

In this chapter the derivation of the equation of motion for a rotor with a massless flexible shaft supported in bearings at its two ends and carrying a rigid disc at its midspan is reviewed. Such a model is popularly known as the 'Jeffeot rotor'. It represents the modal system obtained for any multimass rotor after modal analysis. Internal and external damping are both present in the model. The solution to the equation of motion is presented. The solution is reformatted and the analytical basis for extraction of information about internal and external damping parameters is developed.

2.1 EQUATION OF MOTION

The Jeffcot model for the i-th mode of a rotor is shown in Fig. 2.1. Let x-y-z and ξ-η-z be the stationary and rotating coordinate systems respectively (Fig. 2.2). The geometric centre of the disc is at c and the centre of mass is located at point G. For a rotational speed w the free-body diagram of the disc is described in Fig. 2.3.

The equations of motion can be written as [10,11]

$$m\ddot{x} + (k\xi + h\dot{\xi}) \cos \omega t - (k\eta + h\dot{\eta}) \sin \omega t + c\dot{x} = ma_1 \omega^2 \cos \omega t - ma_2 \omega^2 \sin \omega t \qquad (2.1)$$

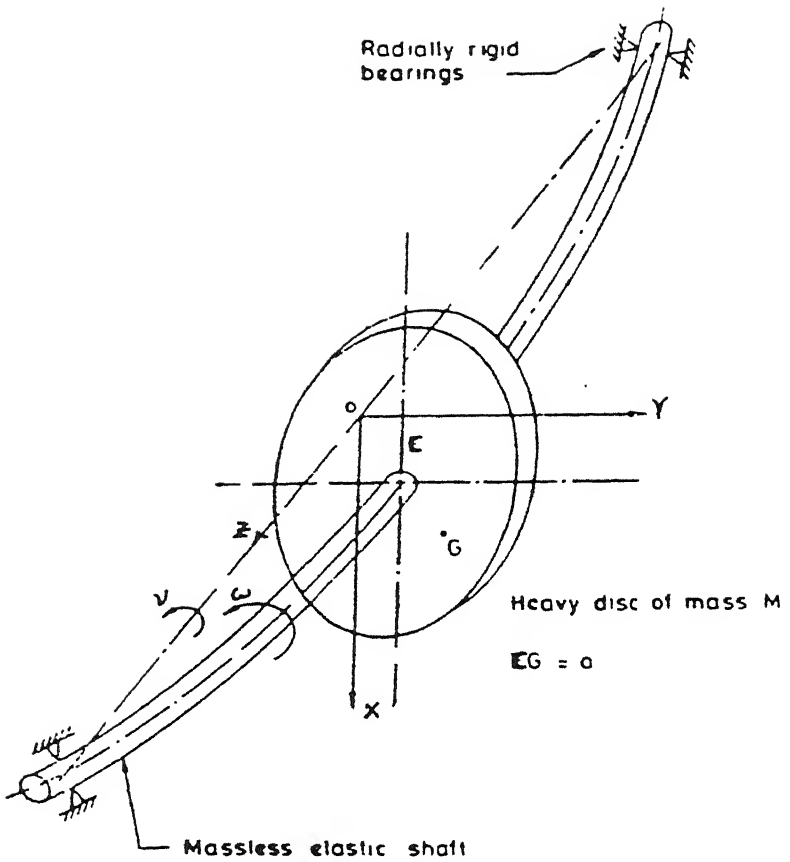

Fig. 2.1 The Jeffcot Model for the i^{th} Mode of a Rotor

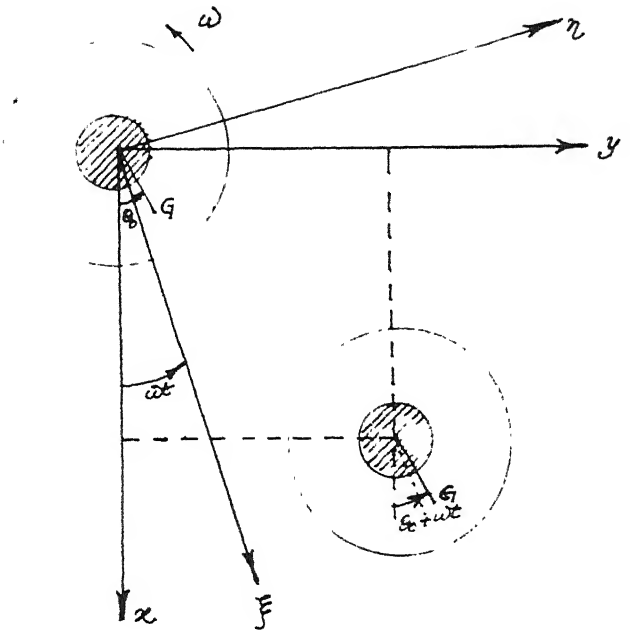

Fig. 2.2 The Stationary and Rotating Coordinate Systems

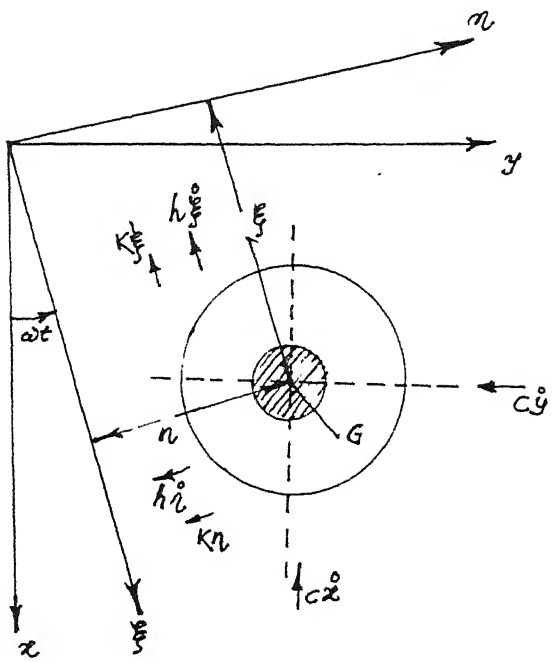

Fig. 2.3 Free Body Diagram of the Disc

$$m\ddot{y} + (k\xi + h\dot{\xi}) \sin \omega t + (k\eta + h\dot{\eta}) \cos \omega t + c\dot{y}$$
$$= m a_1 \omega^2 \sin \omega t - m a_2 \omega^2 \cos \omega t \qquad (2.2)$$

where, $a_1 = a \cos \theta_o$, $a_2 = a \sin \theta_o$ (2.3)

Defining radial vectors $r = x + iy$, $\zeta = \xi + i\eta$ and noting that $r = \zeta e^{i\omega t}$ equations (2.1) and (2.2) can be combined into

$$\ddot{r} + 2C_e \dot{r} + 2C_i (\dot{r} - i\omega r) + p^2 r = a_1 \omega^2 e^{i\omega t} + i a_2 \omega^2 e^{i\omega t} + mg \qquad (2.4)$$

In the above

$$C_e = \frac{c}{2m}; \quad C_i = \frac{h}{2m} \text{ and } p^2 = \frac{k}{m} \qquad (2.5)$$

2.2 SOLUTION OF EOM

The free vibration response of the above equation can be taken as

$$r = A \exp(i\lambda t) \qquad (2.6)$$

Substitution of (2.6) in (2.4) gives

$$\lambda^2 - 2i\lambda (C_e + C_i) - p^2 + 2i\omega C_i = 0 \qquad (2.7)$$

yielding,

$$\lambda_{1,2} = i (C_e + C_i) \pm [\, p^2 - (C_e + C_i)^2 - 2i\omega C_i \,]^{1/2}$$

Defining the damped natural frequency, $P_d^2 = P^2 - (C_e + C_i)^2$, one gets

$$\lambda_{1,2} = i (C_e + C_i) \pm [\, P_d^2 - 2i\omega C_i \,]^{1/2}$$
$$= i (C_e + C_i) \pm [\, (P_d - \frac{i\omega C_i}{P_d})^2 + (\frac{\omega C_i}{P_d})^2 \,]^{1/2}$$

Since C_i is a small quantity ignoring the term $\left(\frac{\omega C_i}{P_d}\right)^2$, one gets

$$\lambda_{1,2} = \pm P_d + i \left(C_e + C_i \mp \frac{\omega C_i}{P_d}\right) \tag{2.8}$$

Hence the solution becomes;

$$r = R_1 \exp\left[-\left(C_e + C_i - \frac{\omega C_i}{P_d}\right) t\right] \exp\left(+ iP_d t\right)$$

$$+ R_2 \exp\left[-\left(C_e + C_i + \frac{\omega C_i}{P_d}\right) t\right] \exp\left(- iP_d t\right) \tag{2.9}$$

For stability of the response (2.9) it is essential that

$$C_e + C_i > \frac{\omega C_i}{P_d} \tag{2.10}$$

It can be seen that the rotor will be stable at

$$\omega < P_d \left(1 + \frac{C_e}{C_i}\right) \tag{2.11}$$

2.3 EXTRACTION OF DAMPING PARAMETERS (C_e AND C_i) FROM THE RESPONSE

The technique for obtaining the damping parameters C_e and C_i from the free vibration response is formulated below. Rewriting the response of eqn. (2.9)

$$r = R_1 \exp\left[-\left(C_e + C_i - \frac{\omega C_i}{P_d}\right) t\right] \exp\left(+iP_d t\right)$$

$$R_2 \exp\left[-\left(C_e + C_i + \frac{\omega C_i}{P_d}\right) t\right] \exp\left(-iP_d t\right)$$

letting

$$A = \left(C_e + C_i - \frac{\omega C_i}{P_d}\right), \qquad B = \left(C_e + C_i + \frac{\omega C_i}{P_d}\right)$$

and since

$r = x + iy$, $R_1 = X_1 + i\,Y_1$ and $R_2 = X_2 + i\,Y_2$

equation (2.9) can be written as

$$r = (X_1 + iY_1)\, e^{-At} (\cos P_d t + i \sin P_d t) + (X_2 + iY_2)\, e^{-Bt} (\cos P_d t + i \sin P_d t) \quad (2.12)$$

Separating the real and imaginary parts, we get

$$x = (X_1\, e^{-At} + X_2\, e^{-Bt}) \cos P_d t + (-Y_1\, e^{-At} + Y_2\, e^{-Bt}) \sin P_d t \quad (2.13)$$

$$y = (Y_1 . e^{-At} + Y_2\, e^{-Bt}) \cos P_d t + (X_1 . e^{-At} - X_2\, e^{-Bt}) \sin P_d t \quad (2.14)$$

In the above it should be noted that X_1, X_2, Y_1 and Y_2 are constants depending on initial conditions.

Differentiating (2.13) and (2.14) with respect to t,

$$\dot{x} = (X_1 . e^{-At} + X_2 . e^{-Bt}) (-P_d \sin P_d t) + \cos P_d t\, (-AX_1 . e^{-At} - BX_2 . e^{-Bt}) + (-Y_1 . e^{-At} + Y_2 . e^{-Bt}) (P_d \cos P_d t) + \sin P_d t\, (AY_1 . e^{-At} - BY_2 . e^{-Bt}) \quad (2.15)$$

$$\dot{y} = (Y_1 . e^{-At} + Y_2 . e^{-Bt}) (-P_d \sin P_d t) + \cos P_d t\, (-AY_1 . e^{-At} - BY_2 . e^{-Bt}) + (X_1 . e^{-At} - X_2 . e^{-Bt}) (P_d \cos P_d t) + \sin P_d t\, (-AX_1 . e^{-At} + BX_2 . e^{-Bt}) \quad (2.16)$$

Let the initial conditions be

$$x = x_o;\quad y = y_o;\quad \dot{x} = \dot{x}_o \text{ and } \dot{y} = \dot{y}_o \text{ at } t = 0.$$

Substituting in equations (2.13) - (2.16) and solving for X_1, X_2, Y_1 and Y_2, we obtain

$$X_1 = \frac{\{(B-A)\,\dot{x}_o + (B^2-AB+2P_d^2)\,x_o + (A+B)\,P_d\,y_o + 2P_d\,\dot{y}_o\}}{[(B-A)^2 + 4\,P_d^2\,]}$$

$$X_2 = \frac{\{-(B-A)\,\dot{x}_o - 2P_d\,\dot{y}_o + (A^2 - AB + 2P_d^2)\,x_o - P_d(A+B)\,y_o\}}{[(B-A)^2 + 4P_d^2]}$$

$$Y_1 = -\frac{\{2\dot{x}_o\,P_d - \dot{y}_o\,(B-A) + x_o\,P_d\,(A+B) - y_o\,(B^2-AB+2P_d^2)\}}{[(B-A)^2 + 4P_d^2]}$$

$$Y_2 = \frac{\{2\dot{x}_o\,P_d - \dot{y}_o\,(B-A) + P_d\,x_o\,(A+B) + y_o\,(A^2-AB+2P_d^2)\}}{[(B-A)^2 + 4P_d^2]}$$

Equations (2.13) and (2.14) can now be written as

$$x = \frac{1}{[(B-A)^2 + 4P_d^2]}\Big[\,[\{(B-A)\,\dot{x}_o + 2P_d\,\dot{y}_o + (B^2-AB+2P_d^2)\,x_o$$

$$+ (A+B)\,P_d\,y_o\}.e^{-At} + \{-(B-A)\,\dot{x}_o - 2P_d\,\dot{y}_o$$

$$+ (A^2 - AB + 2P_d^2)\,x_o - P_d\,(A+B)\,y_o\}.e^{-Bt}]\cos P_d t$$

$$+ [\{2P_d.\dot{x}_o - (B-A)\,\dot{y}_o + P_d\,(A+B)\,x_o$$

$$- (B^2-AB+P_d^2)\,y_o\}.e^{-At} + \{2P_d\,\dot{x}_o - (B-A)\,\dot{y}_o + P_d\,(A+B)\,x_o$$

$$+ (A^2-AB+2P_d^2)\,y_o\}.e^{-Bt}].\sin P_d t\,\Big] \qquad (2.17)$$

$$y = \frac{1}{[(B-A)^2 + 4P_d^2]} \Big[[\{ - 2P_d \dot{x}_c + (B-A)\dot{y}_o - P_d(A+B)x_o + (B^2-AB+2P_d^2)y_o\} .e^{-At} + \{ 2P_d \dot{x}_o - (B-A)\dot{y}_o + P_d(A+B)x_o + (A^2-AB+2P_d^2)y_o\} e^{-Bt}] \cos P_d t + [\{(B-A)\dot{x}_o + 2P_d \dot{y}_o + (B^2-AB+2P_d^2)x_o + P_d(A+B)y_o\} e^{-At} + \{(B-A)\dot{x}_o + 2P_d \dot{y}_o - (A^2-AB+2P_d^2)x_o + P_d(A+B)y_o\} e^{-Bt}] \sin P_d t \Big] \quad (2.18)$$

Expressions (2.17) and (2.18) form a set of nonlinear algebraic simultaneous equations. It can be readily seen that knowing

- the initial conditions x_o, $\dot{x}_o$, y_o, $\dot{y}_o$
- the damped natural frequency pd
- the response x, y after time t,

the equations can be solved for A and B and hence the damping parameters C_e and C_i.

Iterative Newton-Raphson technique in conjunction with experimental investigations can be employed to solve the equations and obtain C_e and C_i.

Starting with assumed values of A and B the resultant response after time t can be calculated from equations (2.17) and (2.18).

Let the response thus calculated be denoted by $\bar{x}$ and $\bar{y}$.

Let the actual response of the system after time t, as obtained from experiment be x and y.

The errors are

$$g_1 = \bar{x} - x$$

and $g_2 = \bar{y} - y$

The errors are minimised using Newton-Raphson technique and corrections dA and dB are sought for the assumptions A and B. These corrections are obtained as

$$dA = \begin{vmatrix} -g_1 & \frac{\partial g_1}{\partial B} \\ -g_2 & \frac{\partial g_2}{\partial B} \end{vmatrix} / \text{Denom.} \quad dB = \begin{vmatrix} \frac{\partial g_1}{\partial A} & -g_1 \\ \frac{\partial g_2}{\partial A} & -g_2 \end{vmatrix} / \text{Denom.}$$

$$\text{where, Donom.} = \begin{vmatrix} \frac{\partial g_2}{\partial A} & \frac{\partial g_1}{\partial B} \\ \frac{\partial g_2}{\partial A} & \frac{\partial g_2}{\partial B} \end{vmatrix} \qquad (2.19)$$

Taking the corrected values of A and B the new assumptions the process can be repeated until the errors fall within specified limits. The detailed expressions for g_1, g_2, $\frac{\partial g_1}{\partial A}$, $\frac{\partial g_1}{\partial B}$, $\frac{\partial g_2}{\partial A}$, $\frac{\partial g_2}{\partial B}$ used in the computational process are given in non-dimensional form in Appendix 1.

CHAPTER III

EXPERIMENTAL INVESTIGATIONS

3.1 THE RIG

A portable rotor rig was fabricated and set up in the laboratory to carry out investigations. The rig is modular in design and can be employed for a variety of experiments on rotors.

The rig consists of a shaft which supported in two identical ball bearings. The bearing housings are mounted in the slots provided in a base frame. Provisions are made in the base frame to carry shafts of different lengths. The shaft diameter can also be varied and corresponding set of bearings can be supported in the same bearing housings. A number of discs can be mounted on the shaft as desired. The shaft is driven by a 50 W AC/DC motor through a flexible coupling. The motor is also mounted on the frame. A variac was used to control the input supply voltage to the motor and hence the rotational speed can be maintained as desired.

To set the rotor into transient whirling motion at any desired rotational speed, the system was inflicted with an impact load. The transient motion can be readily recorded as a decaying plot.

.2 INSTRUMENTATION

The instrumentation Fig. 3.1 consists of two accelerometers ounted on one of the bearing housing to pick up vibrations in he horizontal and vertical directions. The signals from the ccelerometers are magnified in charge amplifiers and passed hrough filters (to filter the signal component with any required requency) and then displayed on a CRO. The CRO is connected to a rinter. In addition an FFT analyser is used for identification f natural frequencies.

The details of rig and instruments are given in Appendix 2. wo rotor configurations are considered

i) Shaft with a single disc at its midspan (Fig. 3.2).
ii) Shaft with two discs with unequal masses along its length (Fig. 3.3).

.3 NATURAL FREQUENCY DETERMINATION

Prior to experimentation for damping determination, the atural frequencies of the system need to be identified. This is ssential in order to filter out the response corresponding to a articular natural mode from the total response of the system as icked up by the accelerometers.

The natural frequencies of the system are experimentally btained by subjecting the system to an impact load using an mpact hammer, so that it is set into free vibration. The free ibration response is displayed on the amplitude vs. frequency

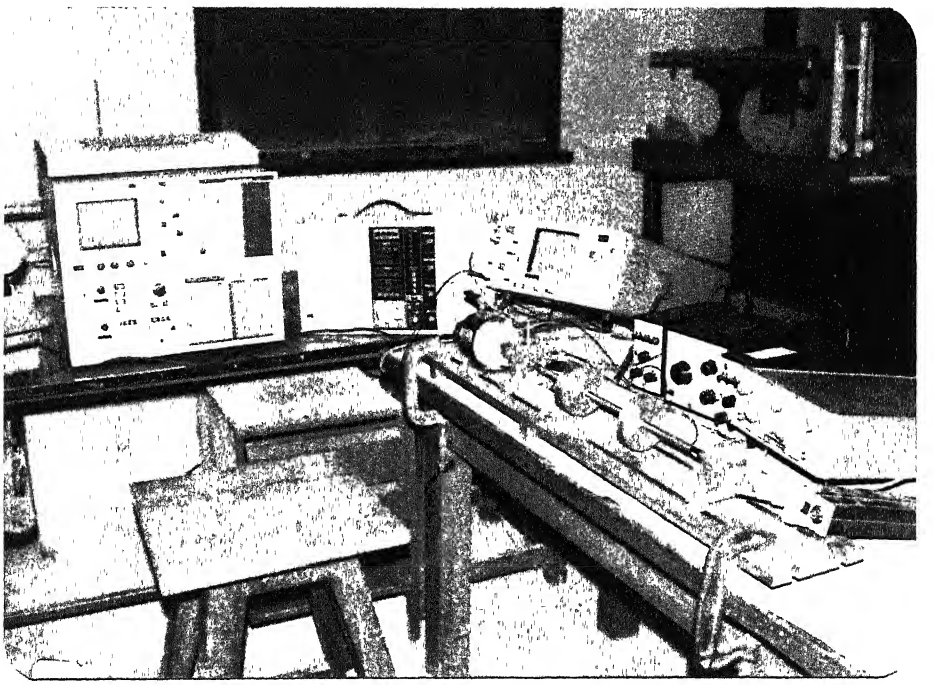

Fig. 3.1 The Experimental Rig with Instrumentation

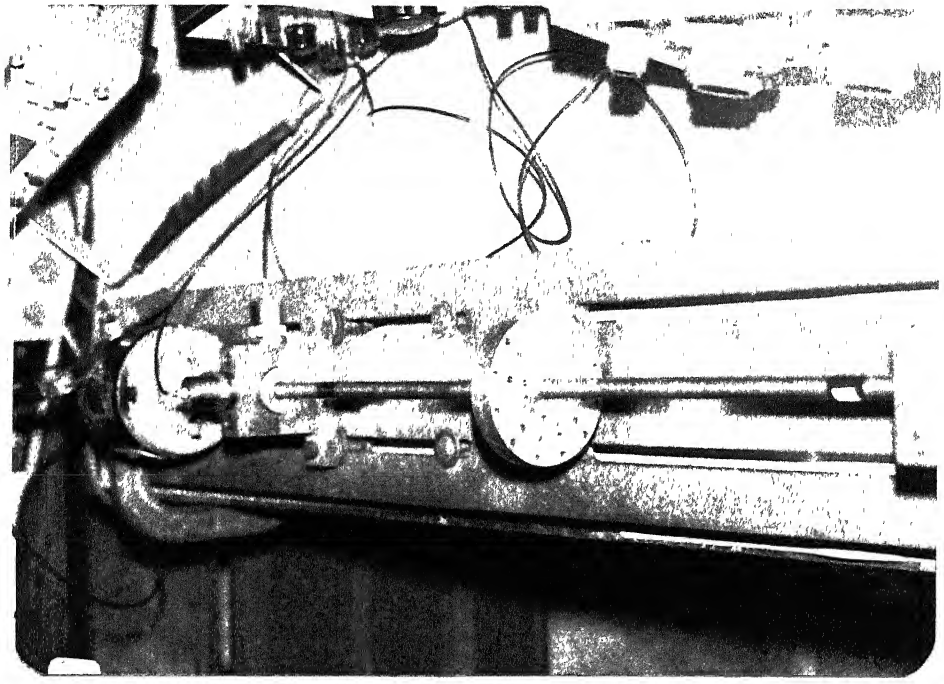

Fig. 3.2 The Rig with Single Mass Rotor

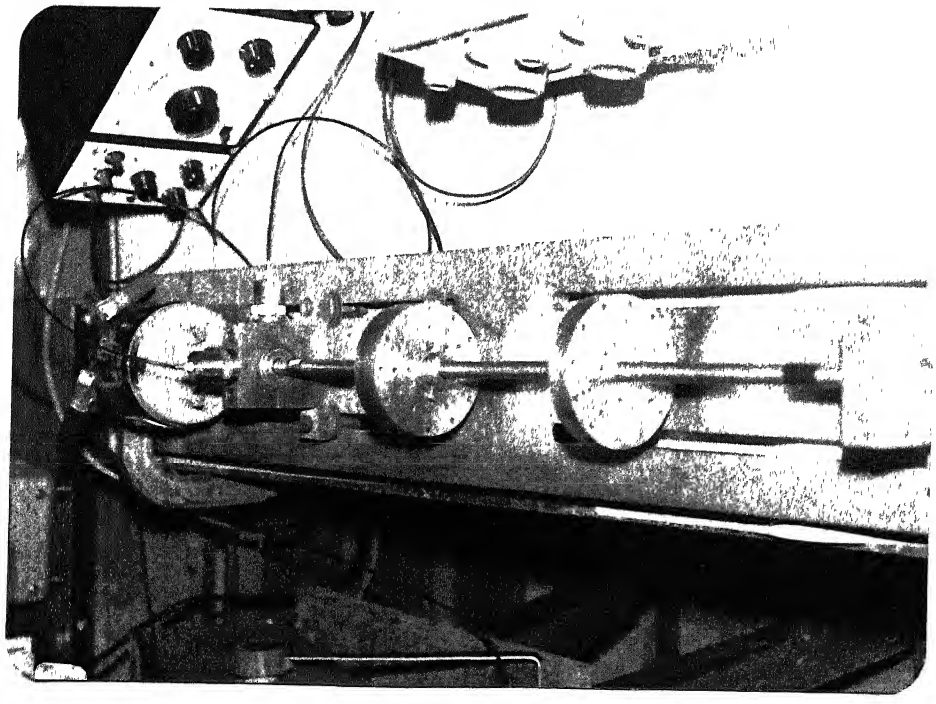

Fig. 3.3 The Rig with Two Mass Rotor

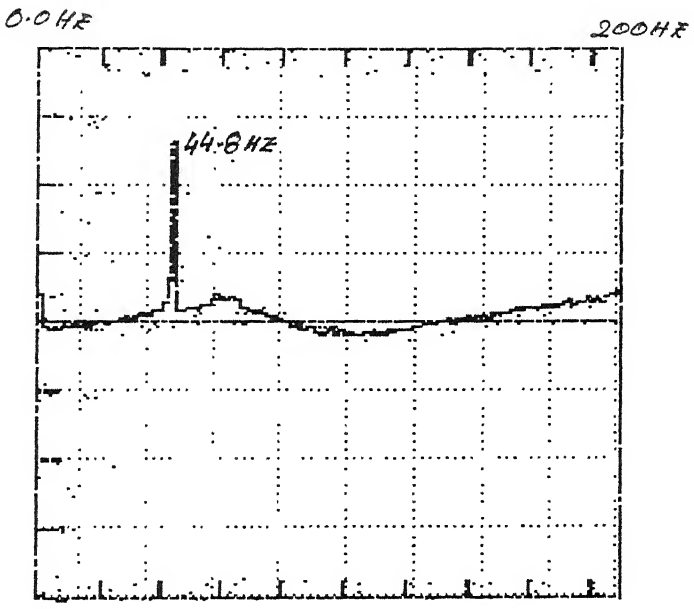

Fig. 3.4 The FFT Plot for Single Mass Rotor

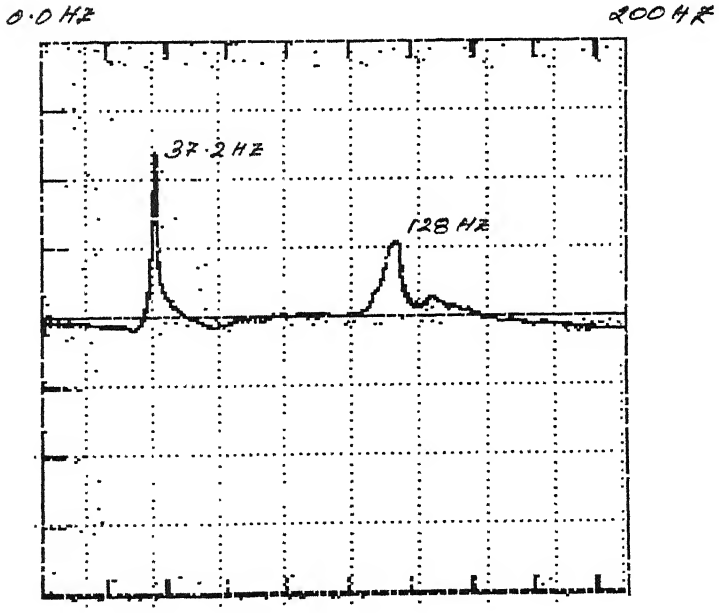

Fig. 3.5 The FFT Plot for Two Mass Rotor

frame of the FFT analyser and the natural frequencies are identified.

Fig. 3.4 shows the FFT plot obtained for a single disc rotor. The natural frequency can be seen to be 44.8 Hz. This value agrees well with the theoretical result obtained as follows.

Idealising the rotor a single degree freedom system the natural frequency is

$$p = \sqrt{\frac{k_{shaft}}{m_{disc}}} .$$

For the configuration under consideration

$$k_{shaft} = \frac{48EI}{L^3} = 39584.067 \text{ kg/sec}^2$$

and $m_{disc} = 0.515$ Kgs.

yielding $p = 44.2$ Hz.

Fig. 3.5 shows the FFT plot for the rotor with two discs. The natural frequencies can be seen to be 37.2 Hz and 128 Hz.

The natural frequencies can be computed theoretically very readily by influence coefficients method for a two degree freedom system.

Referring to Fig. 3.6 the influence coefficient matrix is

$$\begin{bmatrix} \alpha_{11} & \alpha_{12} \\ \alpha_{21} & \alpha_{22} \end{bmatrix}$$

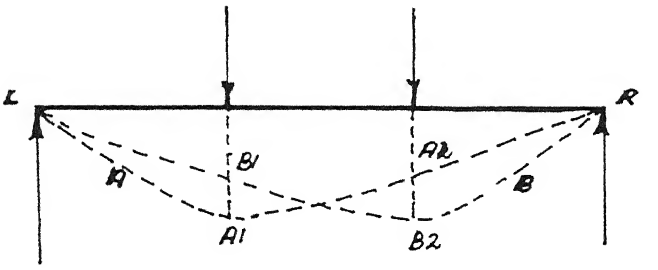

(a) static deflection due to two mass

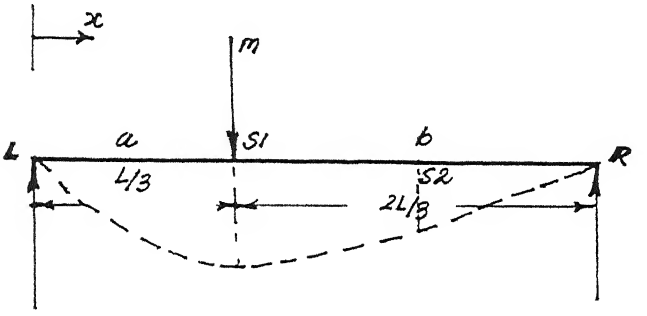

(b) Deflection due to load m at station S1

Fig. 3.6 Influence Coefficients for Static Deflection of Shaft

where $\alpha_{11} = \alpha_{22} = \dfrac{-(8/81)\ L^3}{6\ EI}$

$$\alpha_{21} = \alpha_{12} = \frac{-(7/81)\ L^3}{6\ EI}$$

The natural frequencies are given by [12]

$$P^2_{1,2} = \frac{\alpha_{11}\ m_1 + \alpha_{22}\ m_2 \pm [(\alpha_{11}\ m_1 - \alpha_{22}\ m_2)^2 + 4m_1m_2\ \alpha_{12}^2]^{1/2}}{2\ m_1m_2\ (\alpha_{11}\ \alpha_{22} - \alpha_{12}^2)}$$

The theoretical natural frequencies are thus obtained as 32.5 Hz and 125 Hz and they can be seen to agree well with experiment.

3.4 BALANCING

The rotors need to be balanced before carrying out the investigations. Rigid rotor balancing was done for both the rotor configurations. Nominal amount of balancing was required. The details of balancing are given in Appendix - 3.

3.5 DAMPING DETERMINATION

The technique developed in Chapter 2 requires that starting with a set of initial values x_o, y_o, $\dot{x}_o$ and $\dot{y}_o$ the modal free vibration response x,y of the system be known after time t.

The rotor is run at the desired angular frequency ω by adjusting the motor input voltage. The rotor is then set into free vibrations by inflicting upon it a shock through the impact hammer. The filters are set to the desired natural frequencies so that out of the total system response picked up by the accelerometers only the component corresponding to set natural mode is displayed on the CRO.

The model response recorded simultaneously in the horizontal and vertical directions at a rotor speed of 1200 rpm. are shown in Fig. 3.7 to 3.9. These figures show the time response in the x (vertical) and y (directions) while Fig. 3.10 is a polar plot i.e. x vs. y of the same signal.

It is known that for rotating components damping is not constant but a function of the mode of vibration, speed of rotation and amplitude of vibration [13]. For a particular mode of vibration and speed of rotation, damping will be a function of the amplitude of vibration.

This phenomenon is manifested in the present study as well, as will be seen later from the results.

The iterative damping estimation procedure described in Chapter 2 is carried out for every cycle of decaying vibration signal. The damping being nonlinear in nature, for valid employment of the equation of motion described in the earlier chapter, a practical approximation is made - that for a particular rotor speed and a specific mode of vibration the damping parameters remains practically constant over a cycle of vibration. The damping parameters thus determined are construed to be valid only for the average polar amplitude of vibration during the cycle under consideration. Such approximations have been made in studies concerning rotating turbine blades [14,15] and is considered a pragmatic way of incorporating the dependence of damping on the amplitude of vibration. Hence assuming the damping

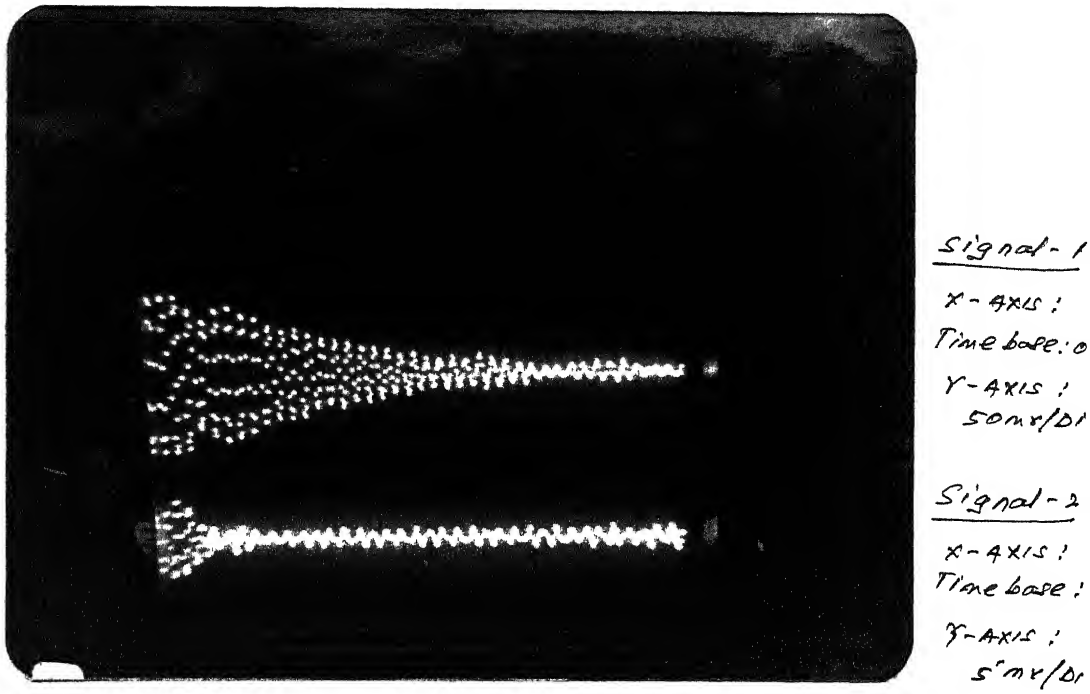

Fig. 3.7 The Frozen Transient Signal in Vertical & Horizontal Directions at 1200 RPM *For Single mass Rotor*

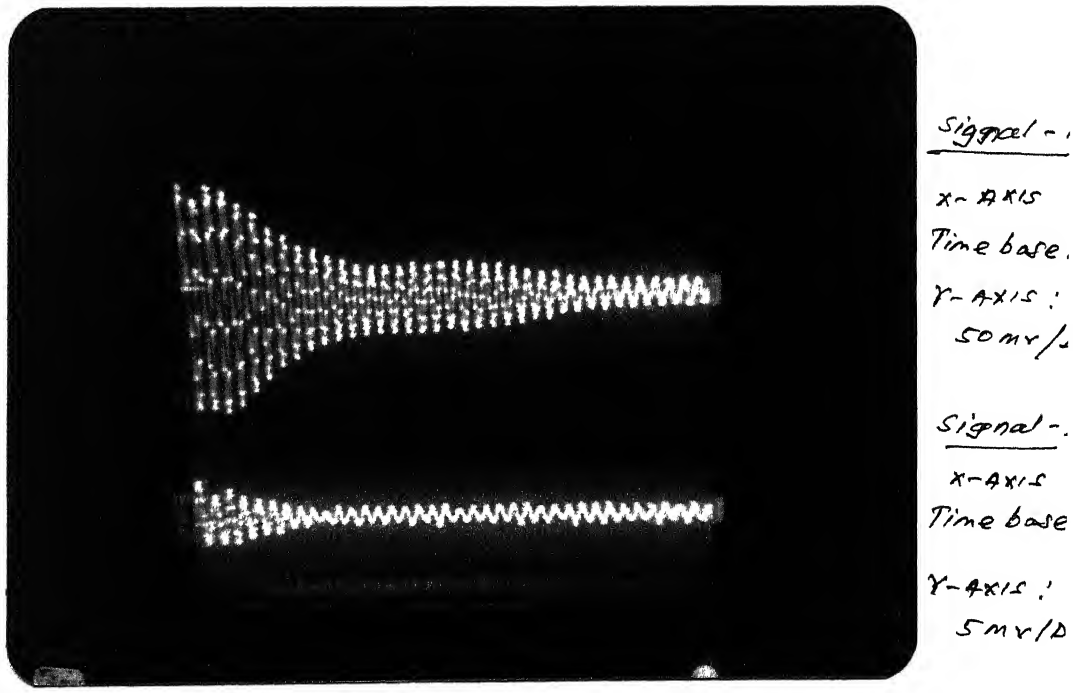

Fig. 3.8 The Frozen Transient Signal in Vertical & Horizontal

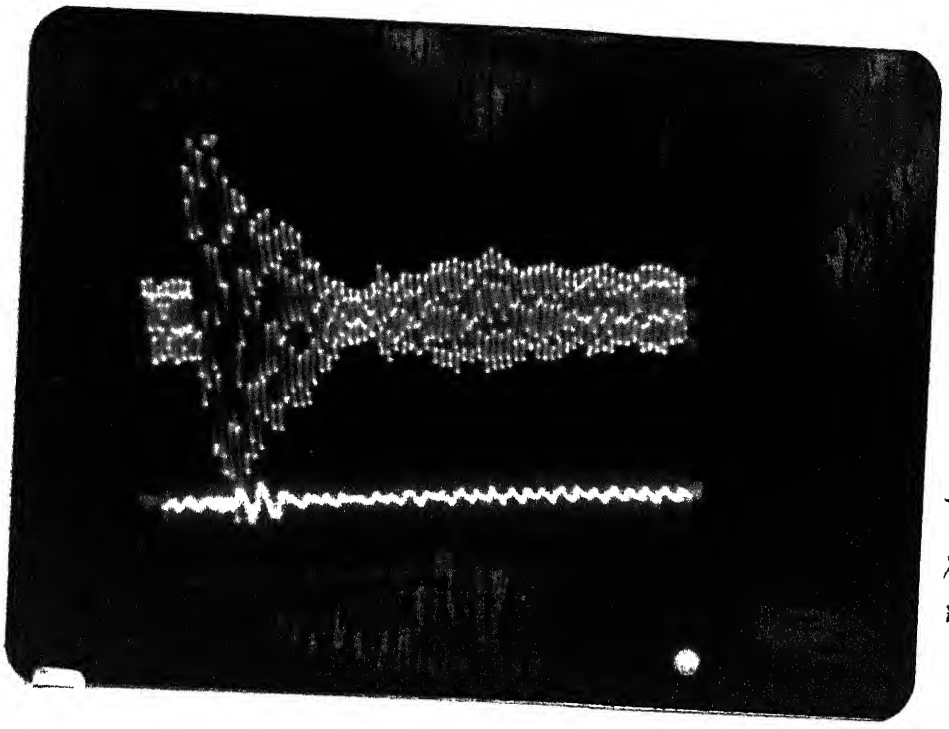

Fig. 3.9 The Frozen Transient Signal in Vertical & Horizontal Directions at 1200 RPM for Two mass rotor (mode-2)

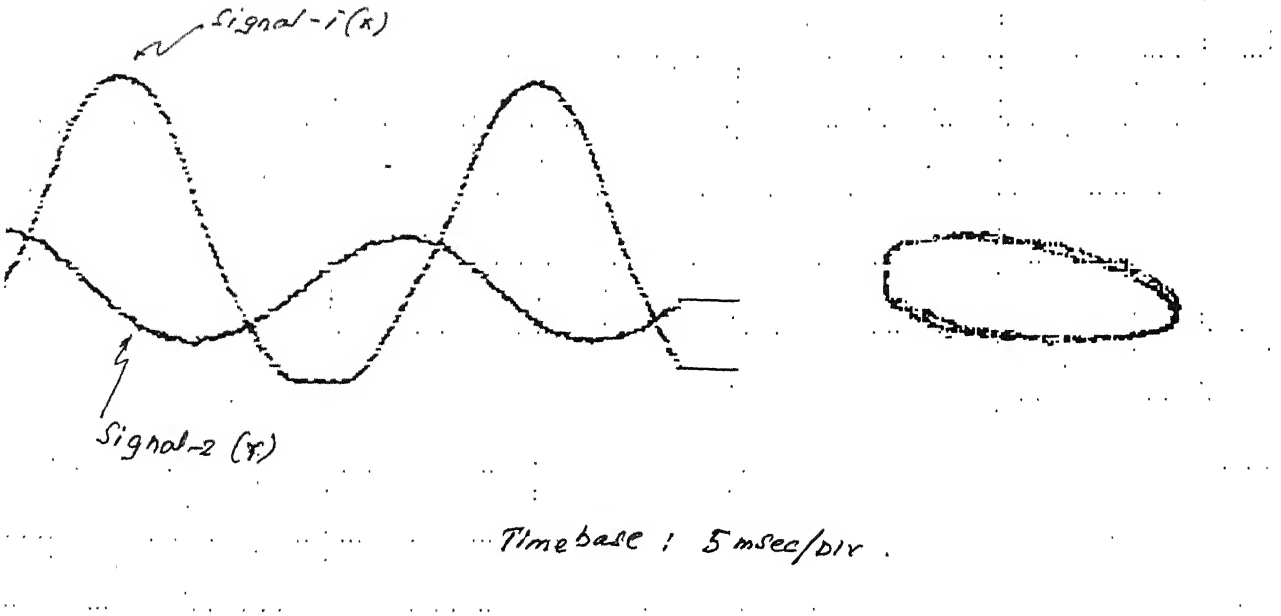

Fig. 3.10 The Polar Plot of the Transient Signal for Single Mass Rotor at 400 RPM

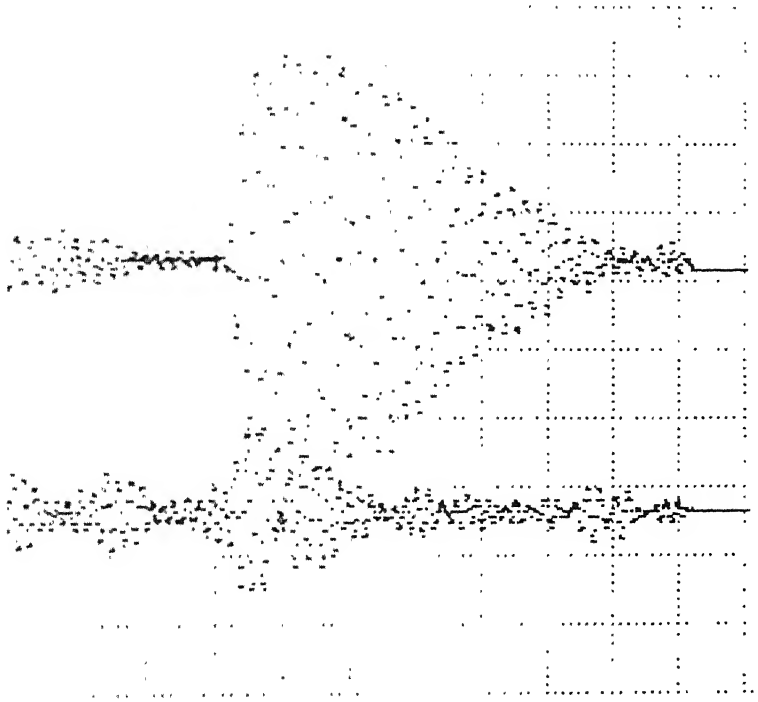

At highly compressed time base of 0.1 Sec/DIV

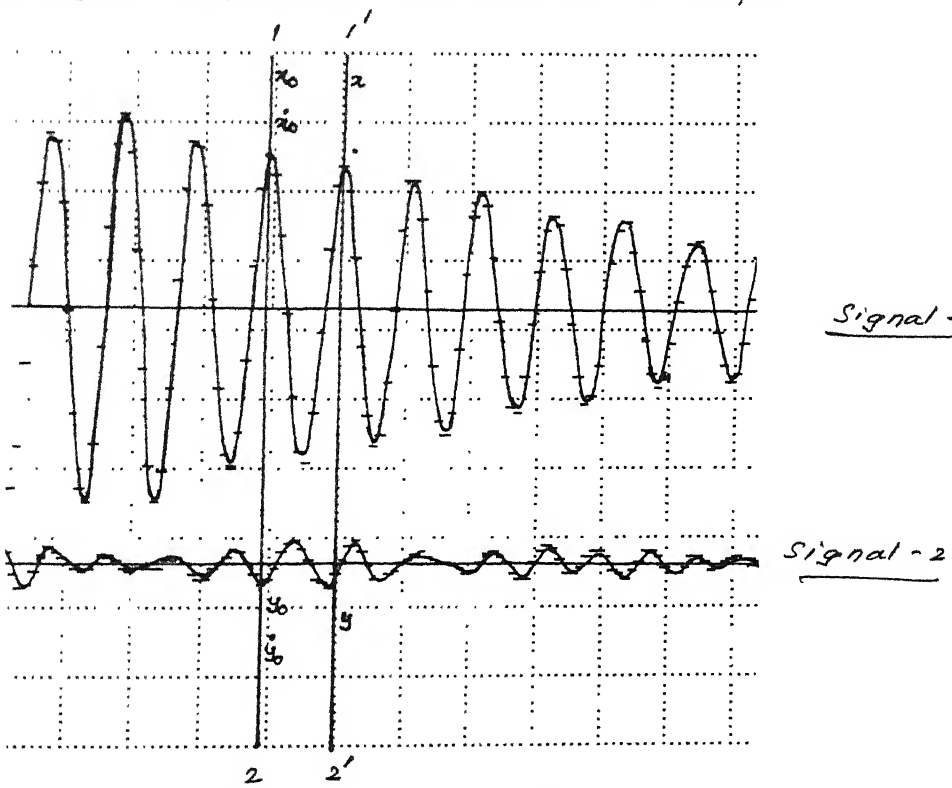

At expanded time base of 5 Sec/DIV

Fig. 3.11 Typical Transient Signal for Single Mass Rotor at 400 RPM

Table 1

$x_o = 0.444$ $\quad \dot{x}_o = 0.0$ $\quad x = 0.402$

$y_o = -0.00135$ $\quad \dot{y}_o = 0.0$ $\quad y = -0.00126$

$p_d = 44.8$ Hz.

Iteration No.	Initial Values				Final Values			
	A	B	Error G_1	Error G_2	A	B	Error G_1	Error G_2
1	0.037028	0.042980	-	-	0.122393	0.157052	-0.1271001	-0.1515828×10^{-3}
2	0.122393	0.157052	-0.1271001	-0.1515828×10^{-3}	0.015193	0.016610	0.00110024	-0.1149175×10^{-3}
3	0.015193	0.016610	0.0110024	-0.1149175×10^{-3}	0.015060	0.016715	0.8350611×10^{-4}	0.9545358×10^{-5}
4	0.015060	0.016715	0.8350611×10^{-4}	0.9545358×10^{-5}	0.015060	0.016715	0.1788139×10^{-6}	-0.8149073×10^{-8}

Final values A = 0.0150607

B = 0.0167158

Hence C_e = 0.4629676

C_i = 0.2488236

i.e. $\zeta_e = \frac{C_e}{p} = 0.0103341$

$\zeta_i = \frac{C_i}{p} = 0.0055541$

parameters as constant over 1 cycle the estimation process is repeated for every cycle of the decaying signal. The damping parameters are then functions of the average polar amplitude during a cycle of vibration.

The damping estimation procedure is detailed in Table 1, for a typical signal (Fig.3.11) at 400 rpm, for the single mass rotor. Damping is evaluated between points 1 and 2, and 1' and 2'.

3.5 RESULTS AND DISCUSSION

Computations as detailed in Table 1 were repeated for five consecutive pair of amplitude in the decay signal. The plots of Amplitude ratio. External damping and Amplitude ratio internal damping for various rotational speeds and modes for the case of rotor with signal mass at the midspan (as shown in Figs. 3.12 to 3.16) and for rotor with two mass equally spaced between the bearings (as shown in Figs. 3.17 to 3.26 were made.

It can be observed from the results that damping is dependent on the amplitude of vibration, rotor speed and the mode of vibration.

For both the rotors it can be seen that the internal damping ζ_i which is attributed to shaft material hysteresis increases with amplitude of vibration. This is in concurrence with the knowledge that material damping in metals increases with the amplitude of vibration.

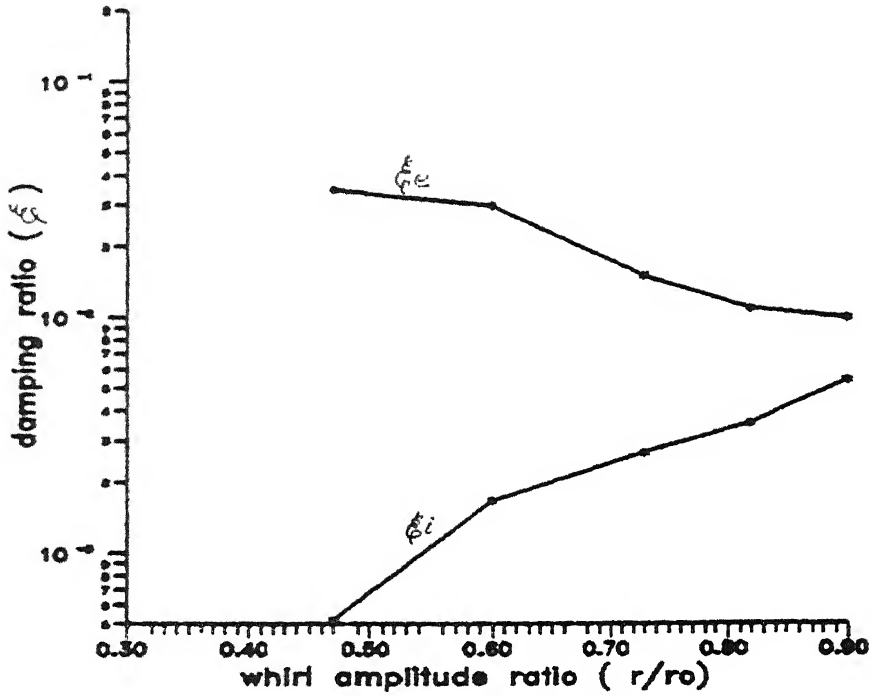

Fig.3.12 Variation of damping with whirl amplitude at 400 rpm for single mass rotor

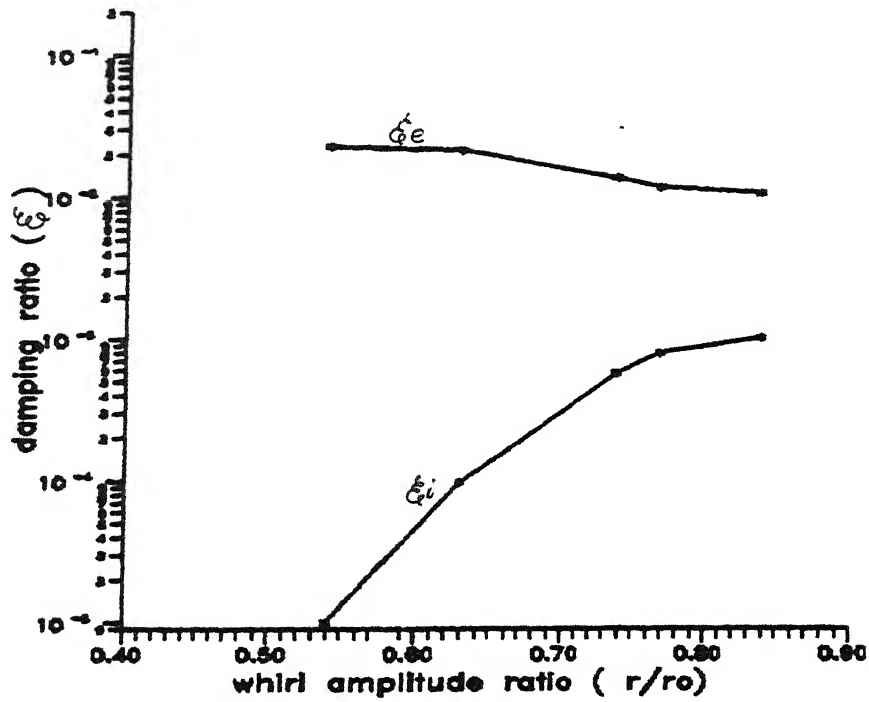

Fig.3.13 Variation of damping with whirl amplitude at 800 rpm for single mass rotor

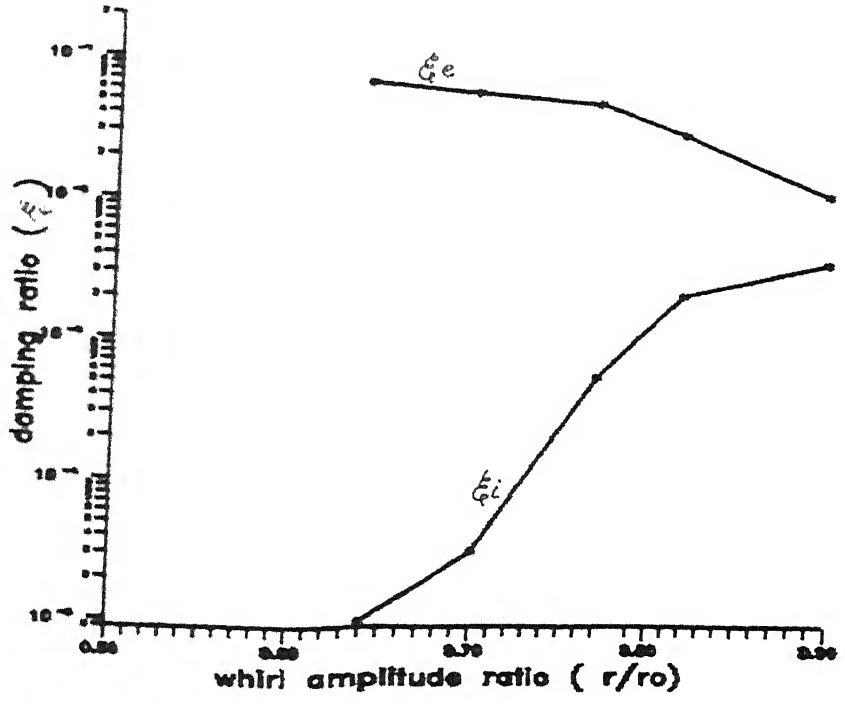

Fig.3.14 Variation of damping with whirl amplitude at 1200 rpm for single mass rotor

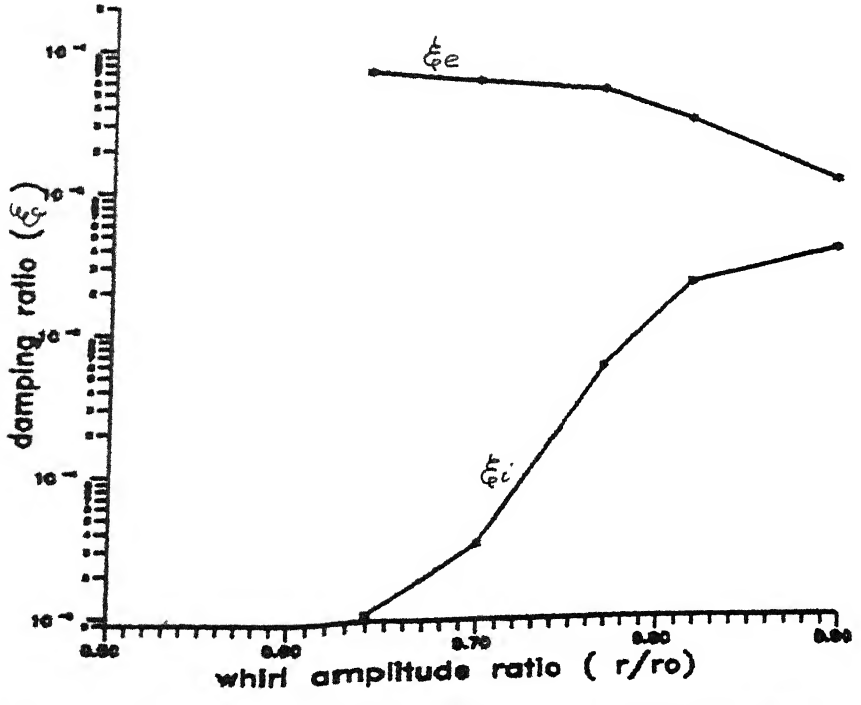

Fig.3.15 Variation of damping with whirl amplitude at 1600 rpm for single mass rotor

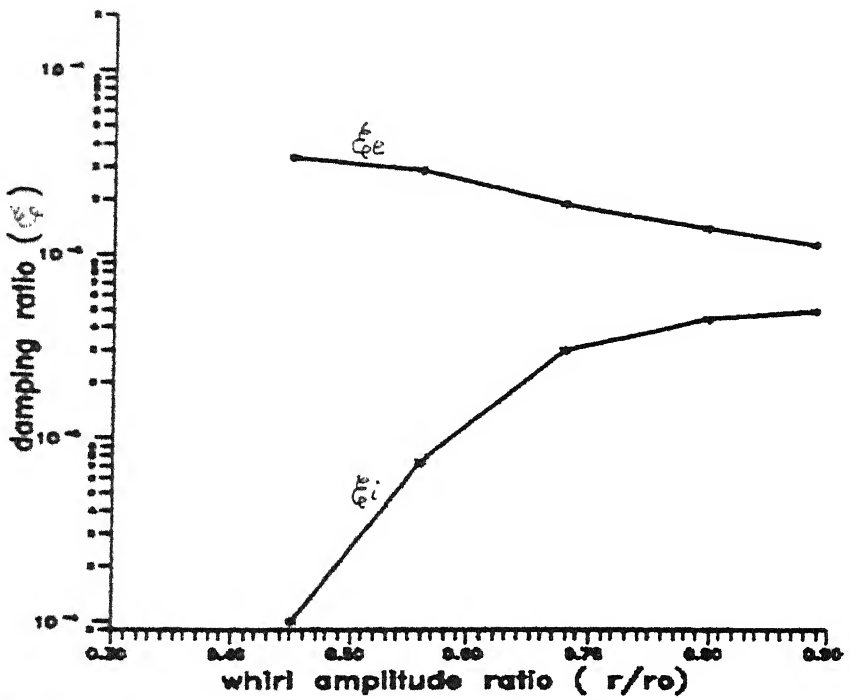

Fig.3.16 Variation of damping with whirl amplitude at 2000 rpm for single mass rotor

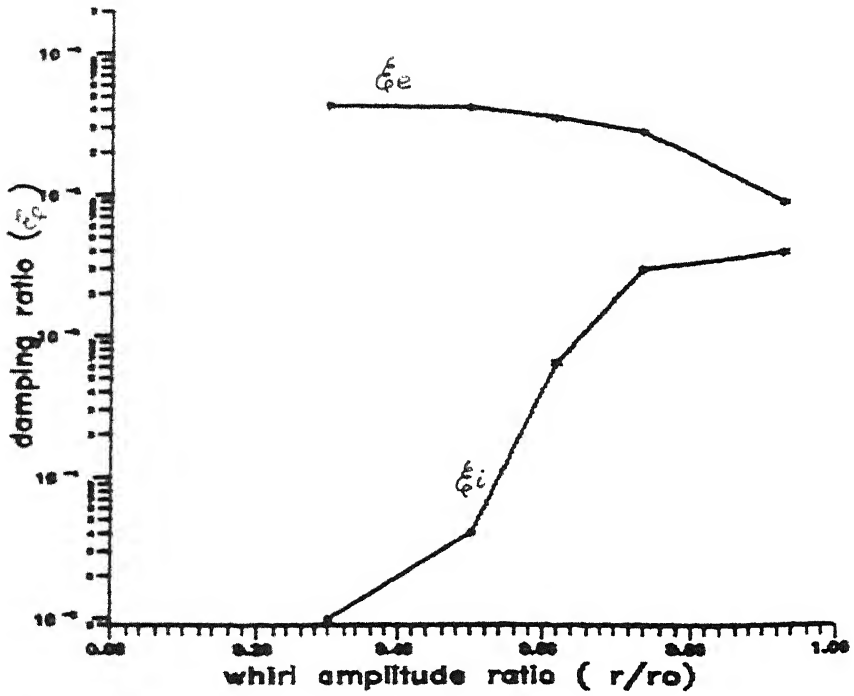

Fig.3.17 Variation of damping with whirl amplitude at 400 rpm for two mass rotor (mode 1)

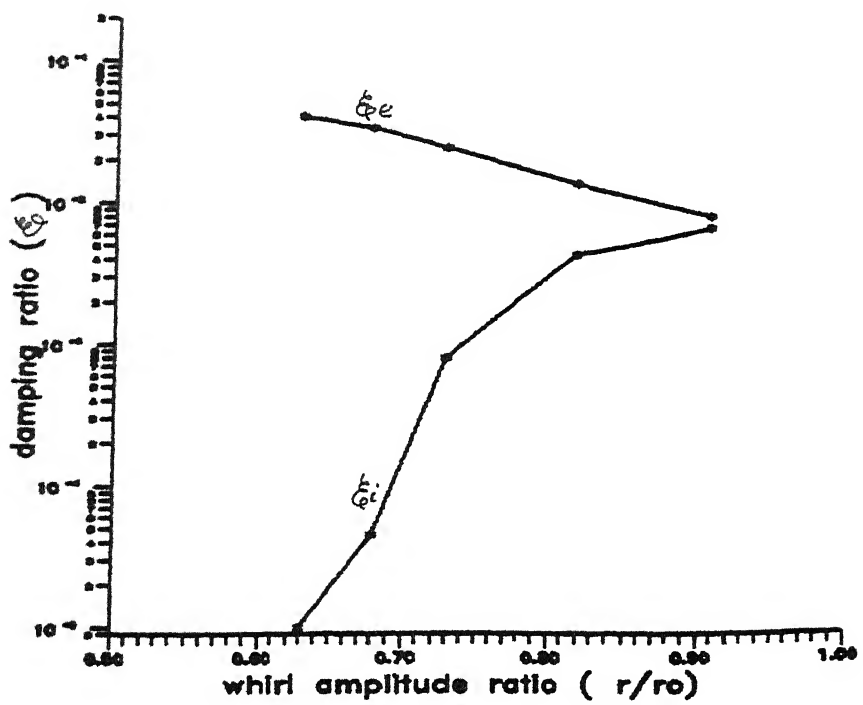

Fig.3.18 Variation of damping with whirl amplitude at 800 rpm for two mass rotor (mode 1)

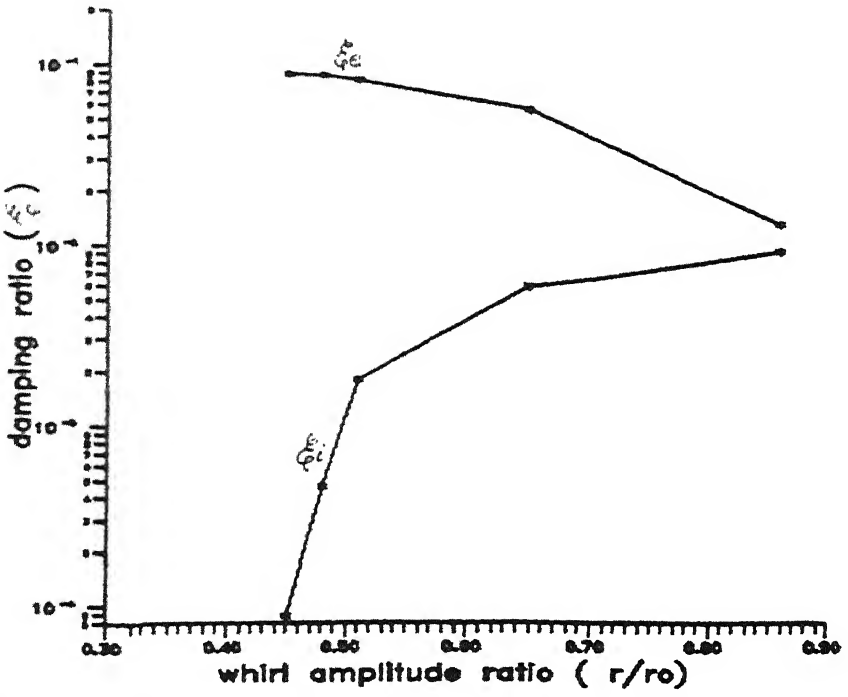

Fig.3.19 Variation of damping with whirl amplitude at 1200 rpm for two mass rotor (mode 1)

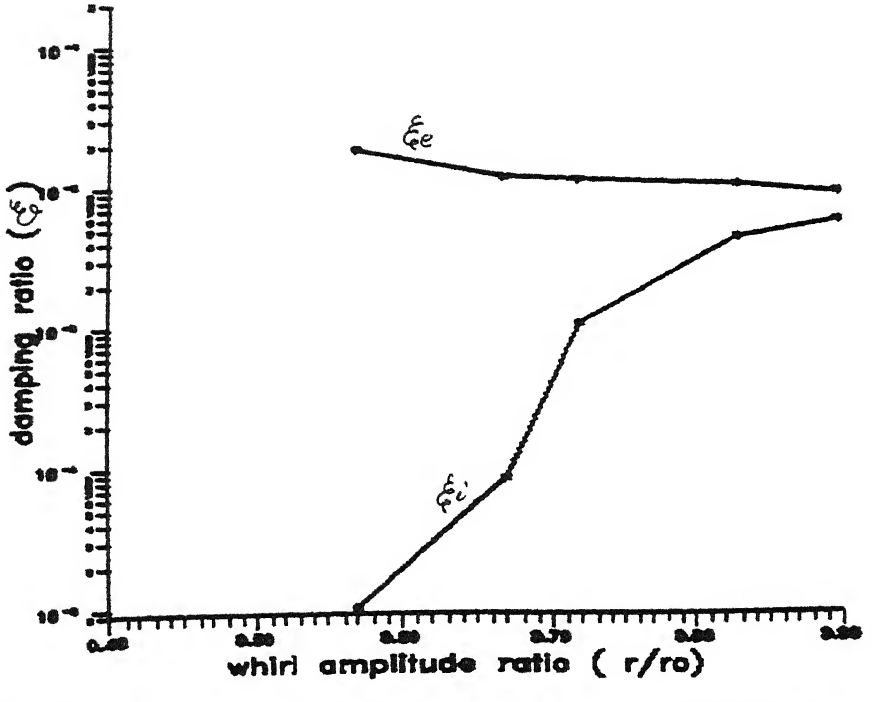

Fig.3.20 Variation of damping with whirl amplitude at 1600 rpm for two mass rotor (mode 1)

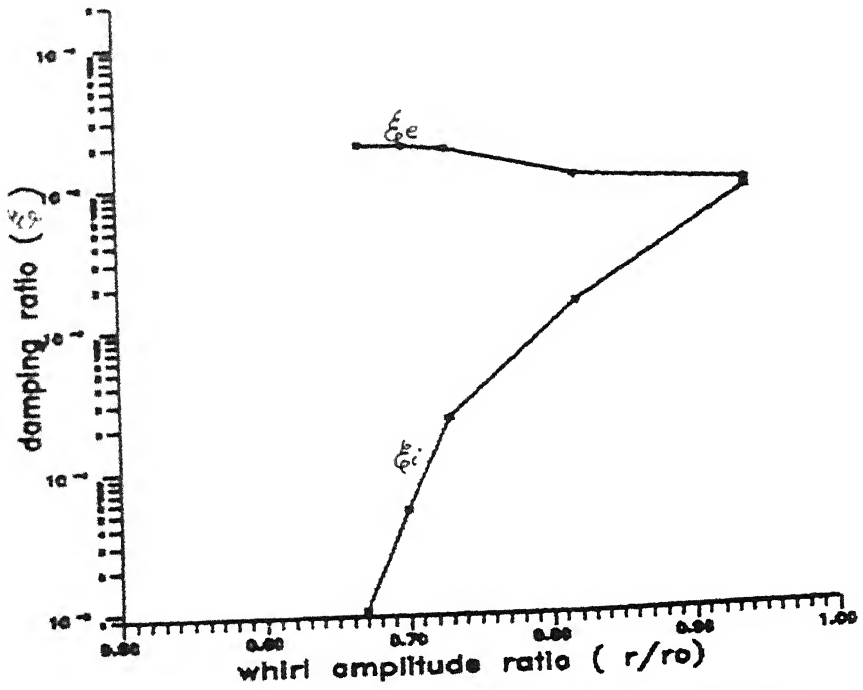

Fig.3.21 Variation of damping with whirl amplitude at 2000 rpm for two mass rotor (mode 1)

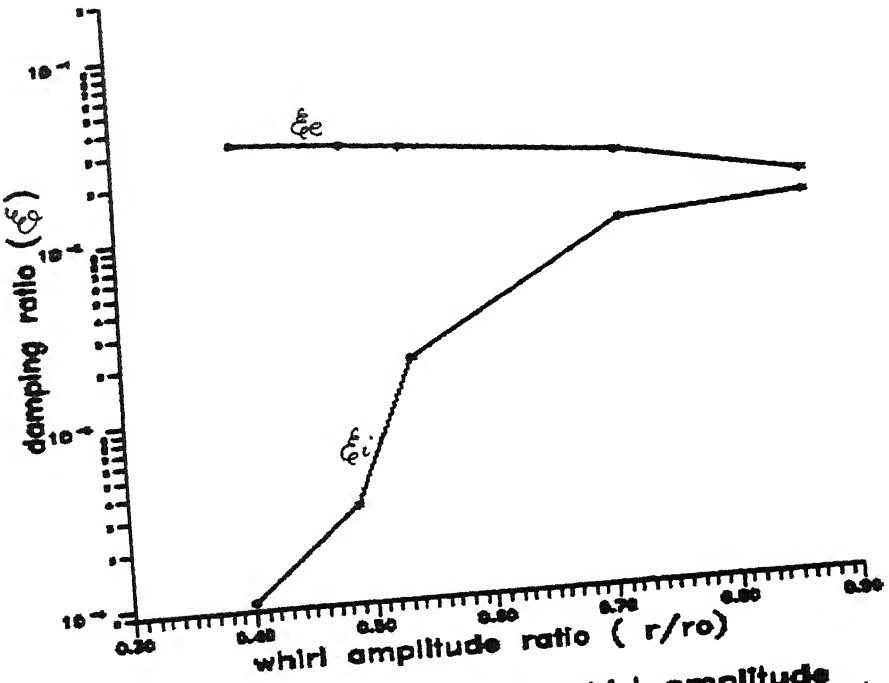

Fig.3.22 Variation of damping with whirl amplitude at 400 rpm for two mass rotor (mode 2)

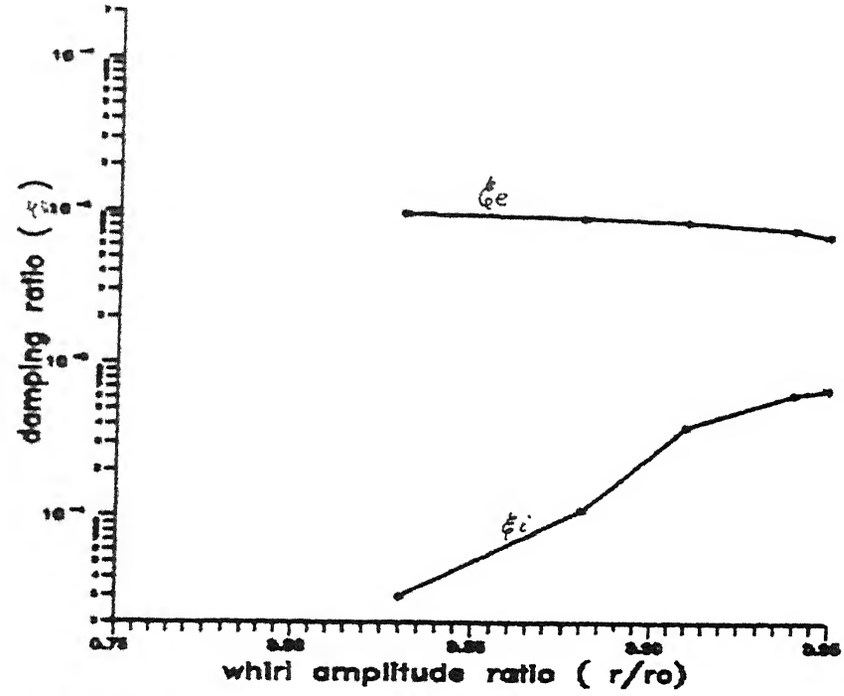

Fig.3.23 Variation of damping with whirl amplitude at 800 rpm for two mass rotor (mode 2)

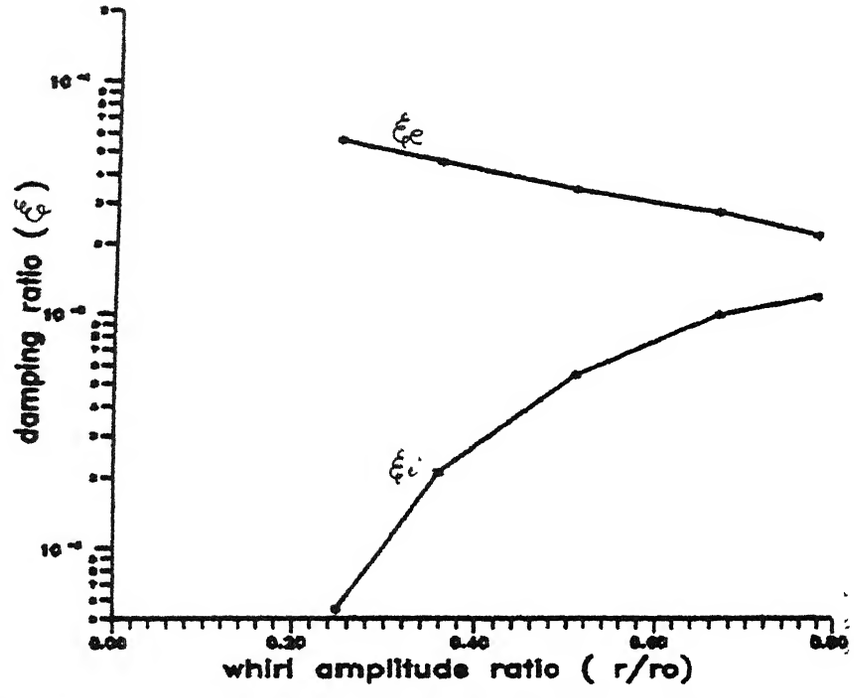

Fig.3.24 Variation of damping with whirl amplitude at 1200 rpm for two mass rotor (mode 2)

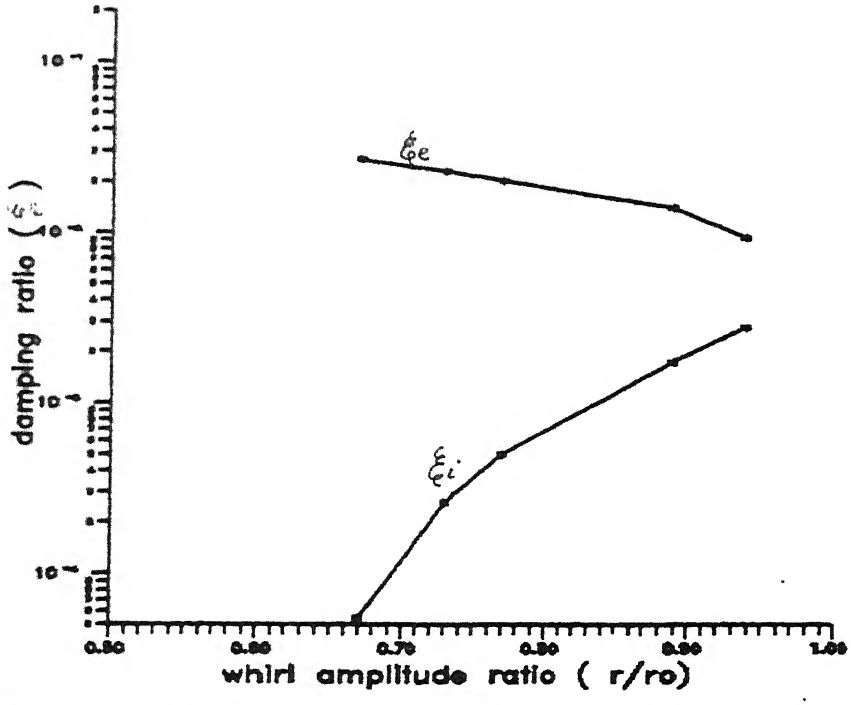

Fig.3.25 Variation of damping with whirl amplitude at 1600 rpm for two mass rotor (mode 2)

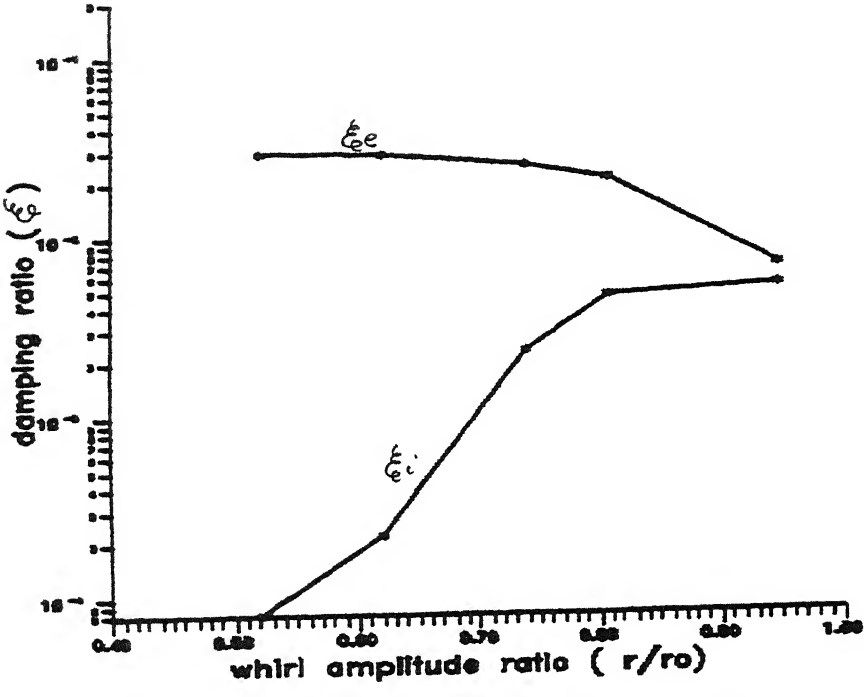

Fig.3.26 Variation of damping with whirl amplitude at 2000 rpm for two mass rotor (mode 2)

The [illegible] due to friction at supports and aerodynamic [illegible] seen to decrease, though not significantly with increasing amplitudes. More investigations under better controlled environment will be required prior to making any conclusion about this phenomenon.

For the two mass system it can be observed that both the external and internal damping values are higher in the second mode. This is in conformity with commonly observed phenomenon that damping is the least in the fundamental mode of vibration.

CHAPTER 4

CONCLUSIONS AND SCOPE FOR FUTURE WORK

This technique for distinguishing between external and internal contributions to damping in rotors has been formulated and established experimentally.

This technique, on application to real life rotors with necessary modifications, can be expected to fill a crucial gap of extracting information about internal and external damping mechanisms separately in rotors.

Once information about internal damping characteristics of a newly manufactured rotor can be known by such a technique it is expected to be an important first step in design of fluid film bearings whereby the bearing damping characteristics (i.e. external damping for the rotor) can be appropriately modelled for better control over rotor dynamics.

The laboratory rig and instrumentation however needs improvement. The present study was constrained by equipment availability. Instead of sensing the vibrations by bearing cap accelerometers, signals would by more appropriately picked up by non-contact type displacement transducers directly overlooking the

shaft. Better filters and amplifiers would also be needed. Shock loads can be inflicted on the rotor in a more controlled manner by using electromagnets. The results are highly sensitive to data. Hence automatic data logging in the computer and processing are imperative.

The rig is modular in design and can be readily employed to study characteristics of composite shafts. Investigations and analytical modelling can be reformatted to study instability and define it in terms of acceptable levels of amplitude disturbances at different rotor speeds.

The technique formulated in the present study needs to be implemented for fluid film bearings. This would be essential in order to establish its significance and practicability to real life rotors.

REFERENCES

[1] Newkirk, B.L., 'Shaft Whipping', General Electric Review, Vol. 27, 1924, p. 169.

[2] Kimball, A.L., 'Internal Friction Theory of Shaft Whipping', General Electric Review, Vol. 17, 1924, p. 244.

[3] Kimball, A.L., 'Internal Friction as a Cause of Shaft Whirling', Vol. 16, 1925, p. 724.

[4] Ehrich, F.F., 'Shaft Whirl Induced by Rotor Internal Damping', Int. of Appl. Mech., June 1964, p. 279.

[5] Enrich, F.F., 'The Dynamic Stability of Rotor/Stator Radial Rubs in Rotating Machinery', Jnl. Engg. for Ind. Trans. ASME, Vol. 91, No. 4, 1969, p. 1025.

[6] Begg, I.C., 'Friction Induced Rotor Whirl - A Study in Stability', Jnl. Engg. for Industries, Trans. ASME, 1974, p. 451.

[7] Bansal, P.N. and Kirk, R.G., 'Stability and Damped Critical Speeds of Rotor-Bearing Systems', Jnl. of Engg. for Ind., Nov. 1975, p. 1325.

[8] Zorzi, E.S. and Nelson, H.D., 'Finite Element Simulation of Rotor Bearing Systems with Internal Damping', Jnl. Engg. for Ind., Trans. ASME, 1977, p. 71.

[9] Glasgow, D.A. and Nelson, H.D., 'Stability Analysis of Rotor-Bearing Systems Using Component Mode Synthesis', Trans. ASME, Vol. 102, April 1980.

[10] Tondl Ales, 'Some Problems of Rotor Dynamics', Chapman and Hall, London, 1965.

[11] Rao, J.S., Rotor Dynamics : Wiley Eastern Limited, 1983.

[12] Rao, J.S., and Gupta, K., 'Introductory Course on Theory and Practice of Mechanical Vibrations', Wiley Eastern Limited, 1984.

[13] Rao, J.S., Gupta, K. and Vyas, N.S., 'Blade Damping Measurements in a Spin Rig with Nozzle Passing Excitation Simulated by Electromagnets', Proc. Shock. Vib. Bull., US Naval Res. Labs., Proc. 56, Pt. 2, 1986, p. 109.

[14] Rao, J.S. and Vyas, N.S., 'Resonant Stress Calculation of A Turbine Blade with Damping as A Function of Rotor Speed and Vibratory Amplitude', ASME 89-GT-27.

[15] Rao, J.S., and Vyas, N.S., 'Transient Stress Response of A Turbine Blade under Non-Linear Damping Effects', ASME 90-GT-269.

APPENDIX 1

The detailed expressions for computational process are as follows :

$$G_1 = \frac{1}{[(B-A)^2+4]} \Big[[\{(B-A)\ \frac{1}{p}\ X_1 + \frac{2}{p}\ Y_1 + (A+B)\ Y_o + (B^2-AB+2)\}.e^{-AT}$$

$$+ \{-(B-A)\ \frac{1}{p}\ X_1 - \frac{2}{p}\ Y_1 - (A+B)\ Y_o + (A^2-AB+2)\}.e^{-BT}].\cos(T)$$

$$+ [\{\frac{2}{p}\ X_1 - (B-A)\ \frac{1}{p}\ Y_1 - (B^2-AB+2)\ Y_o + (A+B)\}.e^{-AT}$$

$$+ \{\frac{2}{p}\ X_1 - (B-A)\ \frac{1}{p}\ Y_1 + (A^2-AB+2)\ Y_o + (A+B)\}.e^{-BT}].\sin(T)\Big] - X$$

or $G_1 = \frac{1}{[(B-A)^2+4]}[d_1]$ (A.1)

$$G_2 = \frac{1}{[(B-A)^2+4]} \Big[\{\frac{2}{p}\ X_1 + (B-A)\ \frac{1}{p}\ Y_1 + (B^2-AB+2)\ Y_o - (A+B)\}.e^{-AT}$$

$$+ \{\frac{2}{p}\ X_1 - (B-A)\ \frac{1}{p}\ Y_1 + (A^2-AB+2)\ Y_o - (A+B)\}.e^{-BT}].\cos(T)$$

$$+ [(B-A)\ \frac{1}{p}\ X_1 + \frac{2}{p}\ Y_1 + (A+B)\ Y_o + (B^2-AB+2)\}.e^{-AT}$$

$$+ \{(B-A)\ \frac{1}{p}\ X_1 + \frac{1}{p}\ Y_1 + (A+B)\ Y_o - (A^2-A+B+2)\}.e^{-BT}].\sin(T)\Big] - Y$$

or $G_2 = \frac{1}{[(B-A)^2+4]}[d_2]$ (A.2)

$$\frac{\partial G_1}{\partial A} = \frac{2(B-A)}{[(B-A)^2+4]^2}\ [d_1]$$

$$+ \frac{1}{(B-A)^2+4} \Big[\{(-TB+TA-1)\ \frac{1}{p}\ X_1 - \frac{2T}{p}\ Y_1 + (-TA - TB+1)\ Y_o$$

$$+ (-TB^2 + TAB-2T-B)\}\ .e^{-AT} + \{\frac{X_1}{p} - Y_o + (2A-B)\}.e^{-BT}].\cos(T)$$

$$+ [\{-\frac{2T}{p}\ X_1 + (TB-TA+1)\ \frac{1}{p}\ Y_1 + (TB^2 - TAB+B^2+2T)\ Y_o$$

$$+ \left(\frac{Y_1}{p} + (2A-B)\, Y_o + 1 \right).e^{-BT}].\sin(T)\Big]$$

(A.3)

$$\frac{\partial G_1}{\partial A} = \frac{2(A-B)}{[(B-A)^2+4]^2}\left[d_1\right]$$

$$+ \frac{1}{(B-A)^2+4}\Big[\{(\frac{X_1}{p} + Y_o + (2B-A)\}.e^{-AT}$$

$$+ \{(TB-TA-1)\,\frac{1}{p}\,X_1 + \frac{2T}{p}\,Y_1 + (TA+TB-1)\,Y_o$$

$$+ (-TA^2 + TAB - 2T - A)\}.e^{-BT}].\cos(T)$$

$$+ [\{-\frac{Y_1}{p} - (2B-A)\}\,Y_o + 1].e^{-AT}$$

$$+ \{-\frac{2T}{p}\,X_1 + (TB-TA-1)\,\frac{1}{p}\,Y_1 + (-TA^2 + TAB-2T-A)\,Y_o$$

$$+ (-TA-TB+1)\}\,.\,e^{-BT}].\sin(T)\Big] \qquad (A.4)$$

$$\frac{\partial G_2}{\partial A} = \frac{2(B-A)}{[(B-A)^2+4]^2}\left[d_2\right]$$

$$+ \frac{1}{(B-A)^2+4}\Big[\{-\frac{2T}{p}\,X_1 + (-TB+TA-1)\,\frac{1}{p}\,Y_1 + (-TB^2-TA.B-2T-B)\,Y_o$$

$$+ (TA+TB-1)\}.e^{-AT} + \{\frac{1}{p}\,Y_1 + (2A-B)\,Y_o + 1\}.e^{-BT}].\cos(T)$$

$$+ [\{(-TB+TA-1)\,\frac{1}{p}\,X_1 - \frac{2T}{p}\,Y_1 + (-TA-TB+1)\,Y_o$$

$$+ (-TB^2 + TAB - 2T-B)\}.e^{-AT}$$

$$+ \{-\frac{1}{p}\,X_1 + Y_o - (2A-B)\}.e^{-BT}].\sin(T)\Big] \qquad (A.5)$$

$$\frac{\partial G_2}{\partial B} = \frac{2(A-B)}{[(B-A)^2+4]^2}\left[\alpha_2\right]$$

$$+ \frac{1}{(B-A)^2+4}\Big[[\{\frac{1}{p}Y_1 + (2B-A)\,Y_o - 1\}.e^{-AT}$$

$$+ \{-\frac{2T}{p}X_1 + (TB - TA - 1)\frac{1}{p}Y_1$$

$$+ (-TA^2+TAB-2T-A)\,Y_o + (-TA-TB+1)\}.e^{-BT}].\cos(T)$$

$$+ [\{\frac{1}{p}X_1 + Y_o + (2B-A)\}.e^{-AT}$$

$$+ \{(-TB+TA+1)\frac{1}{p}X_1 + \frac{2}{p}Y_1 + (-TA-TB+1)\,Y_o$$

$$+ (TA^2-TAB + 2T+A)\}.e^{-BT}].\sin(T)\Big] \qquad (A.6)$$

APPENDIX 2

A. The details of equipment used during experimentation are as follows :

1. Accelerometers

   Make : B & K, Type 4370

   Charge Sensitivity : 10,10/10,20 PC^{-2}

   Frequency Range : upto 25 KHz.

2. Charge Amplifier

   Make : B & K, Type 2635

   Charge input : 10^5 PC Max

   Max Output : 8V (mA) Peak

   Frequency Range : ACC/(0.2 or 2 to 100 KHz),
   Velo (1 or 10 to 10 KHz)
   disp. (1 or 10 to 1 KHz)

3. Conditioning Amplifier

   Make : B & K type 2626

   Charge input : ~ 10^5 pc max.

   Max. output : 10V (10mA) peak.

   Frequency Range : 0.3 Hz to 100 Khz.

4. FFT Analyser Sm 2100B

   Make : I watsu, Japan

   No. of Channels : Two

   Sensitivity : ±0.1 to ±200 V/Full scale.

   Frequency Range : DC to 100 KHz.

5. Vibration meter

Make : B & K Type 2511

Frequency Range : 0.3 Hz to 15 KHz

Accuracy : ±5% absolute

6. Phase Meter

Make : B & K, Type 2976

No. of channels : Two

Rotation freq. Range : 2 Hz to 1 Khz.

Photoelectric tacho. probe : Type MM 012

7. Band Pass Filter

i) Tunable band pass filter

Make : B & K, Type 1621

Input : 1V Rms or 0.2 V Rms

Pass bandwidth : Switchable 3% or 23%

Frequency range : 0.2 Hz to 20 Khz.

ii) Solid State Band pass filter.

Make : KROHN-HITE, USA, Type 3700(R)

Input : ± 7V peak

Pass bandwidth : ±5%

Frequency Range = 0.2Hz to 20 KHz.

8. Storage Oscilloscope

Make : Kikusui, Type DSS 6521, Japan

Sensitivity : 5 mV - 10 V/Div.

No. of Channels : Two

Sweep time mag : 5 times.

9. Memory Hi Recorder

Make : HIOKI, Type 8801, Japan

No. of Channels : Four

Recording method : Thermal

Sensitivity : 10 mV/Div to 5 V/Div.

10. Stroboscope

Make : General Radio, Type : Strobotai 1538-A.

Range : 110 to 150,000 RPM

B. The details of the experimental rig is as below :

1. Motor

Make : Tullu-50 Water pump motor, 50 W

Speed Range : 7000 rpm

2. Base plate

Material : Mild Steel

Dimensions : 1m × 0.145 m × 0.012 m

3. Shaft

Material : Stainless steel

Length (ls) : 0.5m

Diameter (ld) : 0.01 m

Modulus of elasticity (Es) = 2.1 × 10" N/M^2

Density (ρ) = 7800 Kg/m^3

4. Disc

Mass of disc 1 = 0.515 Kg

Mass of dice 2 = 0.755 Kg

5. Coupling

Make : Luvjoy

6. Bearings

Make : SKF

Outer dia. : 30 mm

Inner dia. : 10 mm

APPENDIX 3

RIGID ROTOR BALANCING

The balancing procedures based on the influence coefficients measurement is as follows :

i) Two convenient planes L and R and two measurement planes 'a' and 'b' (bearing locations) are chosen (See. Fig. AF.1). Taking $\bar{L}_1$ and $\bar{R}_1$ as the initial readings of vibration levels measured with phase angle ν_1 and δ_1 respectively at a desired rotational speed.

ii) In the second run, a trial mass $\bar{T}_R$ placed at convenient location in plane R and observations $\bar{L}_2 \angle \nu_2$ and $\bar{R}_2 \angle \delta_2$ at measuring planes 'a' and 'b' were taken. Similarly in the third run, placing the trial mass $\bar{T}_L$ in plane L, $\bar{L}_3 \angle \nu_3$ and $\bar{R}_3 \angle \delta_3$ were measured.

iii) The influence coefficient were obtained as

$$\bar{\alpha}_{bR} = (\bar{R}_2 - \bar{R}_1)/\bar{T}_R \qquad \bar{\alpha}_{bL} = (\bar{R}_3 - \bar{R}_1)/\bar{T}_L$$

$$\bar{\alpha}_{aR} = (\bar{L}_2 - \bar{L}_1)/\bar{T}_R \qquad \bar{\alpha}_{aL} = (\bar{L}_3 - \bar{L}_1)/\bar{T}_L$$

Hence

$$\begin{Bmatrix} \bar{R}_1 \\ \bar{L}_1 \end{Bmatrix} = - \begin{bmatrix} \bar{\alpha}_{bR} & \bar{\alpha}_{bL} \\ \bar{\alpha}_{aR} & \bar{\alpha}_{aL} \end{bmatrix} \begin{Bmatrix} \bar{M}_R \\ \bar{M}_L \end{Bmatrix}$$

The correction mass are obtained as

$$\bar{M}_R = \frac{\bar{L}_1 \, \bar{\alpha}_{bL} - \bar{R}_1 \, \bar{\alpha}_{aL}}{\bar{\alpha}_{bR} \, \bar{\alpha}_{aL} - \bar{\alpha}_{aR} \, \bar{\alpha}_{bL}}$$

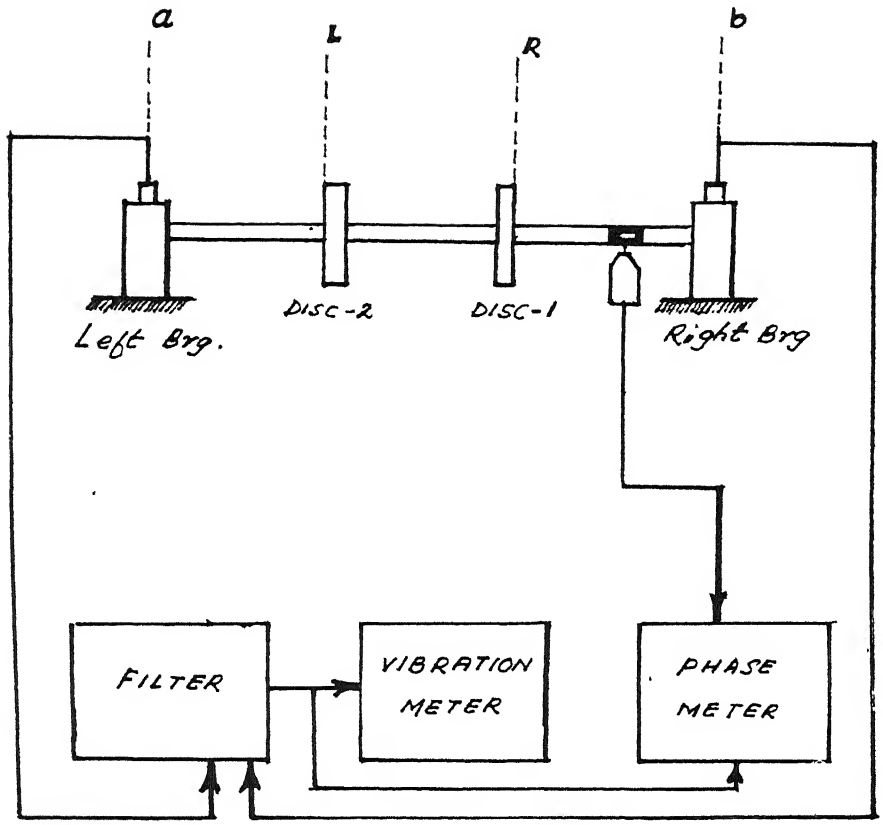

Fig. AF-1 The Block Diagram of Instrumentation Used in Rigid Rotor Balancing

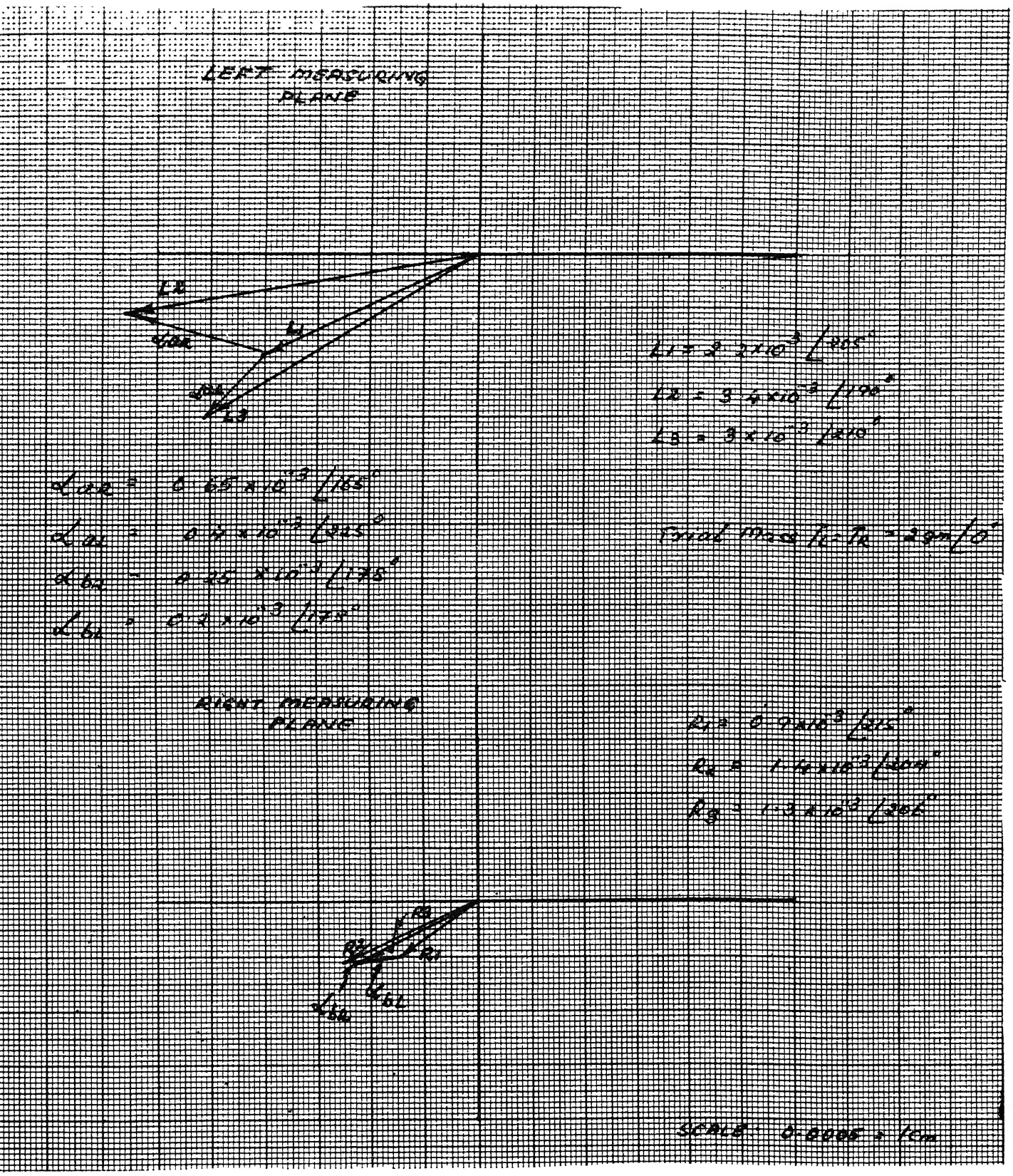

Fig. AF-2 Balancing Measurements for Single Mass Rotor

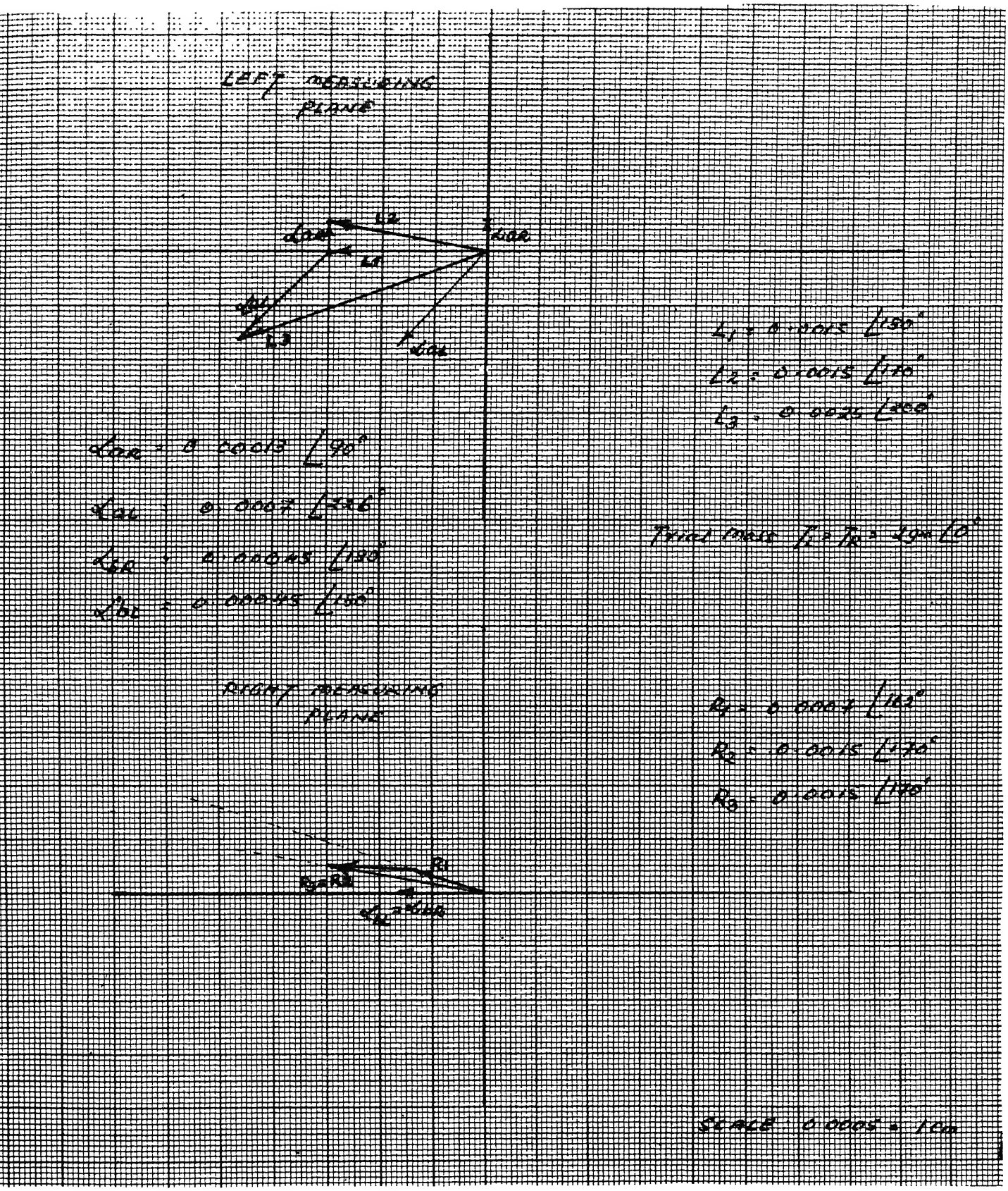

Fig. AF-3 Balancing Measurements for Two Mass Rotor

$$\bar{M}_L = \frac{\bar{R}_1\ \bar{\alpha}_{aR} - \bar{L}_1\ \bar{\alpha}_{bR}}{\bar{\alpha}_{bR}\ \bar{\alpha}_{aL} - \bar{\alpha}_{aR}\ \bar{\alpha}_{bL}}$$

The measured values are represented as vectors as shown in fig. AF.2 and fig. AF.3 for single mass rotor and two mass rotor respectively. The phase angle measurements were done taking positive in the direction of rotation (and negative against the direction of rotation), referring the marked trial mass as 0° in each correction planes.

The correction masses and the residual unbalance obtained are given below,

1. For single mass rotor :

$\bar{M}_R = 3.294$ gms $\angle -143.6^\circ$

$\bar{M}_L = 0.389$ gms $\angle -134.6^\circ$

$\bar{L}_R = 1.2 \times 10^{-3} \angle 204^\circ$

$\bar{R}_R = 0.6 \times 10^{-3} \angle 200^\circ$

2. For two mass rotor :

$\bar{M}_R = 0.887$ gms $\angle -98.6^\circ$

$\bar{M}_L = 1.971$ gms $\angle 134.5^\circ$

$\bar{L}_R = 0.0089 \angle 175^\circ$

$\bar{R}_R = 0.0004 \angle 158^\circ$

The rotors have always some residual unbalance, however well they might be balanced and are considered within tolerable limit.

ERRATA

PTER ①

Page ①, Line 10
Page ②, Line 22 } Read 'junction' for 'function'

APTER ②

Read the following corrected equations.

$$m\ddot{x} + (K_\xi + h\dot{\xi})\cos\omega t - (K\eta + h\dot{\eta})\sin\omega t + c\dot{x} = ma_1\omega^2\cos\omega t - ma_2\omega^2\sin\omega t + g \qquad (2.1)$$

$$m\ddot{y} + (K_\xi + h\dot{\xi})\sin\omega t + (K\eta + h\dot{\eta})\cos\omega t + c\dot{y} = ma_1\omega^2\sin\omega t - ma_2\omega^2\cos\omega t \qquad (2.2)$$

$$\ddot{r} + 2C_e\dot{r} + 2C_i(\dot{r} - i\omega r) + p^2 r = a_1\omega^2 e^{i\omega t} + ia_2\omega^2 e^{i\omega t} + g \qquad (2.4)$$

$$r = R_1 \exp\left[-(C_e + C_i - \frac{\omega C_i}{P_d})t\right]\exp(iP_d t) + R_2 \exp\left[-(C_e + C_i + \frac{\omega C_i}{P_d})t\right]\exp(-iP_d t) \qquad (2.9)$$

$$dA = \begin{vmatrix} -g_1 & \frac{\partial g_1}{\partial B} \\ -g_2 & \frac{\partial g_2}{\partial B} \end{vmatrix} / Denom \qquad dB = \begin{vmatrix} \frac{\partial g_1}{\partial A} & -g_1 \\ \frac{\partial g_2}{\partial A} & -g_2 \end{vmatrix} / Denom .$$

$$Denom = \begin{vmatrix} \frac{\partial g_1}{\partial A} & \frac{\partial g_1}{\partial B} \\ \frac{\partial g_2}{\partial A} & \frac{\partial g_2}{\partial B} \end{vmatrix} \qquad (2.19)$$

Fig : 2.1 The coordinate axes ; be read as

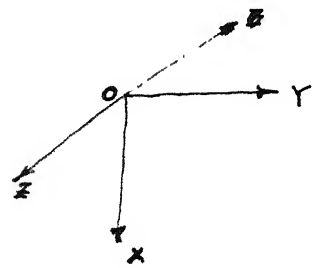

OZ = Brg. centre line.

Read $\overset{\circ}{x_0}$ as $\dot{x}_0$ and $\overset{\circ}{y_0}$ as $\dot{y}_0$

$\overset{\circ}{x}$ as $\dot{x}$ and $\overset{\circ}{y}$ as $\dot{y}$